



Review

Tuning Reconstruction Level of Precatalysts to Design Advanced Oxygen Evolution Electrocatalysts

Hainan Sun ¹, Yinlong Zhu ² and WooChul Jung ^{1,*}

¹ Department of Materials Science and Engineering, Korea Advanced Institute of Science and Technology, Daejeon 34141, Korea; hainansun0718@kaist.ac.kr

² Department of Chemical Engineering, Monash University, Clayton, VIC 3800, Australia; yinlong.zhu@monash.edu

* Correspondence: wcjung@kaist.ac.kr

Abstract: Surface reconstruction engineering is an effective strategy to promote the catalytic activities of electrocatalysts, especially for water oxidation. Taking advantage of the physicochemical properties of precatalysts by manipulating their structural self-reconstruction levels provide a promising methodology for achieving suitable catalysts. In this review, we focus on recent advances in research related to the rational control of the process and level of surface transformation ultimately to design advanced oxygen evolution electrocatalysts. We start by discussing the original contributions to surface changes during electrochemical reactions and related factors that can influence the electrocatalytic properties of materials. We then present an overview of current developments and a summary of recently proposed strategies to boost electrochemical performance outcomes by the controlling structural self-reconstruction process. By conveying these insights, processes, general trends, and challenges, this review will further our understanding of surface reconstruction processes and facilitate the development of high-performance electrocatalysts beyond water oxidation.



Citation: Sun, H.; Zhu, Y.; Jung, W. Tuning Reconstruction Level of Precatalysts to Design Advanced Oxygen Evolution Electrocatalysts. *Molecules* **2021**, *26*, 5476. <https://doi.org/10.3390/molecules26185476>

Academic Editors: Jian Wang, Xin Qian and Hui Kong

Received: 19 July 2021

Accepted: 7 September 2021

Published: 9 September 2021

Publisher's Note: MDPI stays neutral with regard to jurisdictional claims in published maps and institutional affiliations.



Copyright: © 2021 by the authors. Licensee MDPI, Basel, Switzerland. This article is an open access article distributed under the terms and conditions of the Creative Commons Attribution (CC BY) license (<https://creativecommons.org/licenses/by/4.0/>).

Keywords: precatalyst; reconstruction level; surface reconstruction; deep reconstruction; complete reconstruction; OER

1. Introduction

Energy conversion and storage systems are the most promising solutions to address the energy crisis and environmental pollution [1–4]. As a part of these solutions, electrically driven water splitting and the metal-air battery are two representative technologies [5–8]. Due to the complexity of four-electron-proton oxidation, the sluggish kinetics of the OER in electrocatalysis greatly hinders the overall efficiency of these processes [9–13]. Currently, noble metals and their compounds are considered state-of-the-art electrocatalysts for the OER [9,14–21]. To reduce the use of noble metals and ensure better utilization of noble-metal atoms, optimizing emerging design strategies, such as structural engineering, alloying with transition metals, and developing single-atom noble-metal sites are necessary [16,20–22]. Meanwhile, noble-metal-based electrocatalysts are greatly limited when used in commercial applications due to their scarcity and high cost. Therefore, tremendous efforts have been devoted to the development of efficient OER catalysts that cost less [17,23–30].

Particularly, first-row transition metal-based materials, such as oxyhydroxides, oxides (e.g., spinel oxides and perovskite oxides), and metal phosphides/chalcogenides reportedly show outstanding OER performance, given their flexible electronic structure and enriched active sites [31–41]. Notably, the electrocatalytic activities of many reported compounds based on nonprecious transition metals are even superior to those of noble-metal-based catalysts [23,42–45]. To ensure rational designs of precatalysts (catalysts under non-reaction conditions), numerous strategies, such as surface/defect/strain engineering, heteroatom doping, alloying, and the construction of hybrids (e.g., core-shell structure), and

nanoparticle-support composites have been widely developed, by which active sites can be precisely modulated [1,24,42,46–52]. In addition, electro-derived surface reconstruction also plays a significant role in determining electrocatalytic activities [51,53–60]. Advanced in situ/operando techniques have demonstrated that the surfaces of precatalysts tend to be converted partly or completely to oxyhydroxides during the electrochemical oxidation process, acting as actual active species for OER [46,51,61–65]. Although typical in situ-formed species are metal oxyhydroxides for after a reconstruction process, the generated active species can show diverse activities even for the same metal oxyhydroxides, as confirmed by different observed electrocatalytic activities from identical oxyhydroxides on different precatalysts surface [62,66]. This phenomenon further highlights the critical role of the rational design precatalysts.

Furthermore, metal-dissolution-induced reconstruction does not always confer a benefit to electrocatalytic activity. The unintended loss of metal ions from the host lattice often seriously sacrifices the surface crystal configurations to form metal oxyhydroxides with dielectric properties on the catalyst surface, leading to the loss and collapse of the material crystalline matrix [67]. Taking $\text{Ba}_{0.5}\text{Sr}_{0.5}\text{Co}_{0.8}\text{Fe}_{0.2}\text{O}_{3-\delta}$ (BSCF) as an example, this is a benchmark OER material for perovskite oxides in alkaline media [68]. A descriptor predicting intrinsic OER reactivity through the e_g -filling of a perovskite oxide was successfully proposed by Shao-Horn et al. and is now widely used by many researchers. However, it is not easy clearly to determine the degree of e_g -filling on the catalyst surface, and most attempts thus far have been measured through bulk-sensitive analysis techniques or predicted only through calculations of the binding energy values of oxygenated species on the catalyst surface [69]. Importantly, surface reconstruction was not fully considered in the design of the OER response descriptor. The same group later reported an amorphous surface (Co(Fe)OOH phase) of BSCF during the OER process, which explained the initially enhanced activity as determined by cyclic voltammetry and potentiostat measurements [70,71]. These works promoted a further understanding of catalyst surface changes under electrochemical potentials, especially by what are known as in situ/operando techniques [50,51,61,72–76]. It is also important to note that further data from electrochemical experiments revealed that BSCF would lose its superior activity after long-term testing, which is more likely due to the collapse of the crystalline matrix on the surface [77]. Our understanding of surface reconstruction has grown progressively and become more refined with the ongoing research. Therefore, a limitation/circumvention strategy and the acceleration of the surface reconstruction process appear to be other effective methodologies that can be used to design high-performance OER electrocatalysts.

The intent of this review is to summarize recent advances in design strategies for the controllable levels of structural self-reconstruction to develop advanced OER electrocatalysts (Figure 1). We discuss original contributions to the structural self-reconstruction research and the necessity to control surface changes, after which we summarize recently proposed concepts to boost electrocatalytic performance. The challenges and outlooks in this field are also presented in an effort to clarify the current state of surface reconstruction technology and rational designs of high-performance electrocatalysts for the OER.

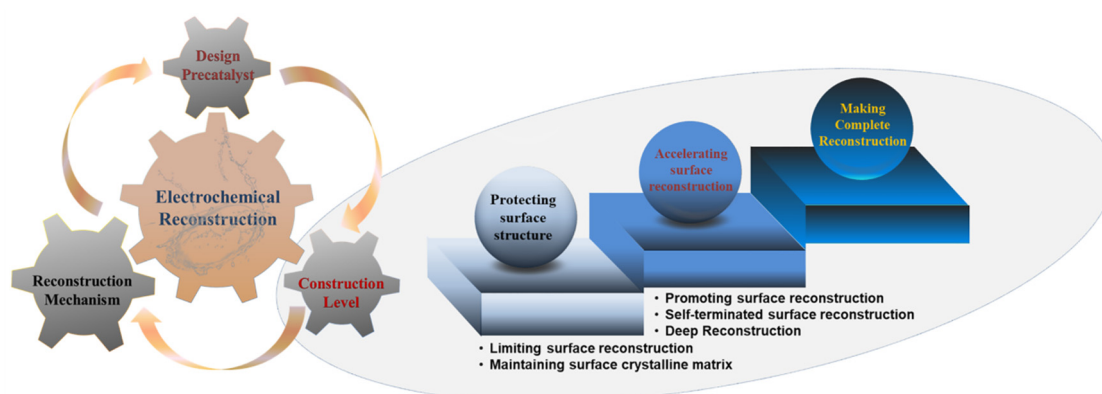


Figure 1. Schematic diagrams of strategies used to control the surface reconstruction process for advanced OER electrocatalysts.

2. Fundamental Understanding of Surface Reconstruction

To gain an in-depth understanding of surface reconstruction coupled with changes in electrocatalytic activity level, it is essential to understand the reaction mechanism of the OER. The equilibrium potential of the OER is 1.23 V vs. a reversible hydrogen electrode at room temperature [26]. The traditionally followed adsorbate evolution mechanism involves different OER intermediates, including HO^* , HOO^* , and O^* species [1,10,65]. The scaling relationships, in which the adsorption energies of different intermediates are linearly correlated, cause the practically applied potential to drive the OER process much higher than the ideal value of 1.23 V [47]. Furthermore, potentials between the applied value in a practical catalytic process and the redox potential of the given catalyst overlap to some extent, which contributes to the occurrence of electrocatalytic activity and catalyst surface structural self-reconstruction at the same time (Figure 2) [53,63,78,79].

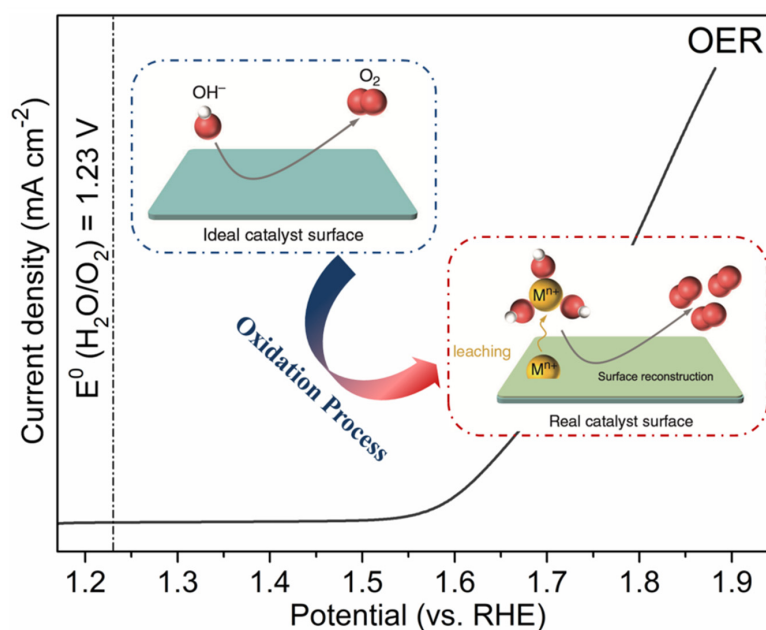


Figure 2. Schematic of the polarization curves of the OER and schematic illustration of the surface reconstruction process. Reproduced with permission [67]. Copyright 2020, Nature Publishing Group.

The structural properties of in situ-formed species on a catalyst surface mainly determine the final catalytic behavior related to the local electronic structure of the species, such as hydrophilicity, co-ordination, and metal-oxygen covalency [55,80]. Recently, a series of sophisticated in situ/operando characterizations have led to the monitoring of the dynamic structural reconstructions of various types of electrocatalysts [61,63,81,82]. These

efforts found that typical in situ-formed species on catalyst surfaces are metal oxyhydroxides [53,62,78,79,82–84]. However, the generated surface-active species showed a range of activity even for the same metal oxyhydroxides, a finding also confirmed by the different observed electrocatalytic activities from identical oxyhydroxides on different precatalysts surfaces [62]. These results further highlight the importance of elaborately designing controllable structures of precatalysts. In addition, factors that affect the reaction conditions such as the concentration of the electrolyte, the applied potential, and the temperature will also affect the degree of surface change [56,85]. Thus, much effort has been devoted to exploring advanced OER electrocatalysts based on surface reconstruction [63,79,86,87].

3. Necessity to Control Surface Reconstruction

Based on the above-mentioned descriptions, surface reconstruction is an ubiquitous electrochemical phenomenon during the OER process [78,79]. However, surface reconstruction engineering is a comprehensive and complex process, which requires the rational design of the precatalyst and precise control of the surface change process [7,63,88]. The parameters of phase/electronic/geometrical structures, oxidation/spin states, and the morphology should be systemically considered [53,79,89–93]. Furthermore, in situ/operando spectroscopic techniques are crucial to identify the actual active species, providing greater insights into the relationship between the structure and activity of the studied catalysts [45,75,82,87,94–98].

Therefore, how rationally to control the surface change, including the rate and level of surface reconstruction, during the OER process to design high-performance OER electrocatalysts is an open question. Herein, to demonstrate the feasibility of this concept, current developments, and recently proposed strategies to boost electrocatalytic performance capabilities by limiting/circumventing/accelerating surface reconstruction processes are discussed below.

4. Protecting Surface Structure

4.1. Limiting Surface Reconstruction

Due to the moderate capacity of binding oxygen, noble-metal oxide RuO_2 is considered as a benchmark OER electrocatalyst, especially in acidic media [9,21,99]. However, the operational stability of RuO_2 is a serious issue to be overcome [90,99]. Great efforts have been devoted to improving the stability of RuO_2 through various types of strategies, such as introduction of heterogeneous elements, strain engineering, and construction of strongly coupled RuO_2 /non-noble-metal hybrids [20,90,99–101]. The deterioration mechanism of RuO_2 is ascribed to the over-oxidation of Ru due to the oxidation of lattice oxygen. The generation of oxygen vacancies caused Ru atoms to be exposed on the catalyst surface, which are then further oxidized to soluble materials (e.g., high-valence-state material RuO_4) (Figure 3a) [9,102]. Surface reconstruction at the expense of the surface crystal structure harms the operational stability [102]. Therefore, it would be reasonable to mitigate this unfavorable surface change if the formation energy of oxygen vacancies is much greater than the redox $\text{H}_2\text{O}/\text{O}_2$ energy. Based on this design concept, Hao et al. utilized a foreign doping strategy to enlarge the localized gap between O $2p$ band centers and the Fermi level, which can enhance the energy barrier for lattice oxygen oxidation and effectively prohibit oxygen vacancies (Figure 3b,c) [102]. The introduction of Er and W into the lattice of RuO_2 modulates its electronic structure. The density of states from density functional theory (DFT) calculations suggests that the gap between O $2p$ band centers and the Fermi level was enlarged from -3.31 eV (RuO_2) to -4.12 eV ($\text{W}_m\text{Er}_n\text{Ru}_{1-m-n}\text{O}_{2-\delta}$), indicating that the covalency of the Ru-O bond was decreased by the co-doped effect. Thus, the reaction mechanism of the $\text{W}_{0.2}\text{Er}_{0.1}\text{Ru}_{0.7}\text{O}_{2-\delta}$ catalyst in an acidic solution would tend to follow the adsorbate evolution mechanism rather than the lattice oxidation mechanism because it is thermodynamically unfavorable for direct O-O coupling of O $2p$ states with regard to the Fermi level (Figure 3a). In addition to the obviously enhanced activity, in terms of the overpotential and current densities (Figure 3d), the co-doped effect can also lead to a

considerable number of active sites exposed on the catalyst surface (Figure 3e). Moreover, the dissolution of metal cations (especially Ru cations) would be successfully suppressed, as revealed by the relatively low and stable concentrations of the dissolved cations in the solution (Figure 3f). The $W_{0.2}Er_{0.1}Ru_{0.7}O_{2-\delta}$ catalyst could survive in highly oxidative and corrosive conditions for at least 350 h, highlighting its superior operational stability.

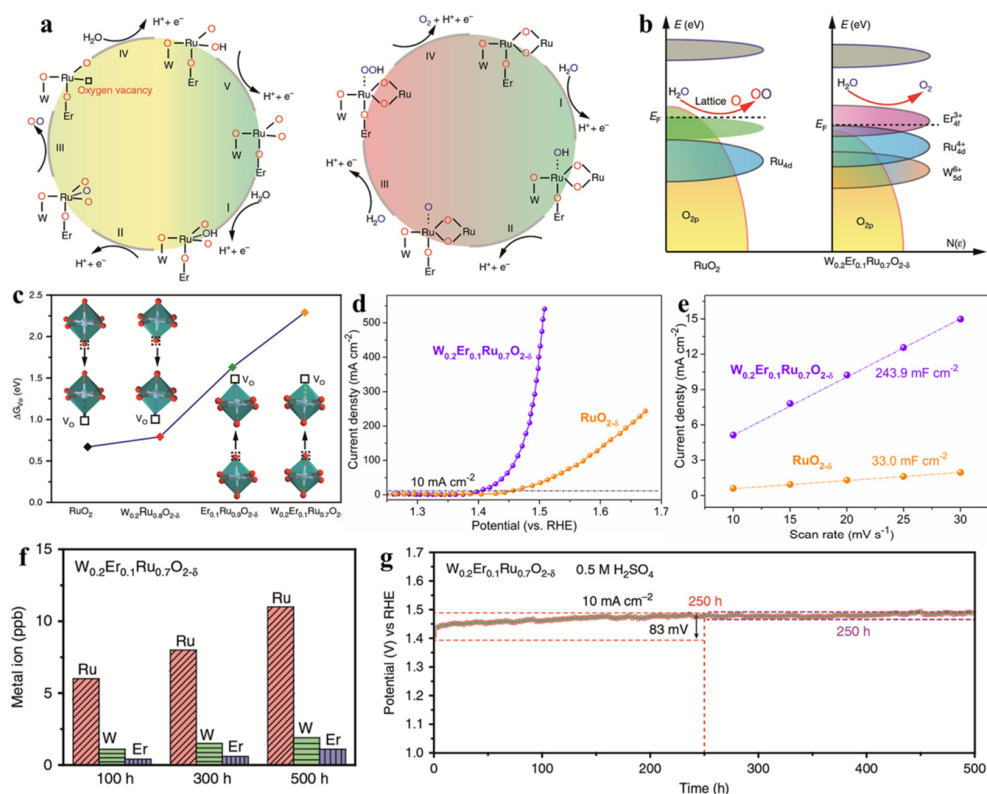


Figure 3. (a) OER reaction mechanisms of LOM and AEM for RuO₂ in acidic media. (b) Schematic diagrams of the band model for RuO₂ and co-doped RuO₂ for the OER in acidic media. (c) Calculated oxygen vacancy formation energy at different positions of RuO₂, single-doped RuO₂, and co-doped RuO₂. (d) LSV curves of RuO₂ and co-doped RuO₂ for the OER in a 0.5 M H₂SO₄ solution. (e) Linear fitting of the capacitive current densities vs. CV scan rates for RuO₂ and co-doped RuO₂. (f) Metal ion dissolution during the OER process. (g) Stability tests for the co-doped RuO₂ catalyst. Reproduced with permission. [102] Copyright 2020, Nature Publishing Group.

4.2. Maintaining Surface Crystalline Matrix

The OER reaction is an oxidation process, during which low-valence metal sites tend to be oxidized to higher valence states along with metal dissolution into the electrolyte [17,53,92,93,98]. Following this, surface reconstruction occurs at the expense of the loss and collapse of the surface crystalline matrix with the formation of an amorphous (oxy)hydroxide layer on the surface [103–105]. In contrast, transition-metal ions with high valence states (e.g., Co³⁺/Co⁴⁺ couples and Fe⁴⁺ ions) can relieve the electro-derived oxidation process and exhibit good structural/operational stability levels, as demonstrated with recently reported high-performance oxides, such as SrCoO₃, Na_{0.67}CoO₂, Ba₄Sr₄(Co_{0.8}Fe_{0.2})₄O₁₅, and CaCu₃Fe₄O₁₂ [26,106–109]. In addition, regarding perovskite oxides, the leaching of ions (cation leaching and anion leaching) is inevitable during the OER process in both alkaline and acidic media [17,18,79,104,110–112].

Considering these factors, Guan et al. proposed a novel design principle by which to optimize the surface reconstruction process for perovskite oxides. In detail, soluble materials (e.g., SrCl₂ and BaCl₂) were introduced into the perovskite structure with high-valence-state transition-metal ions simultaneously to achieve an optimized cation/anion

leaching effect and to keep the surface crystalline matrix unchanged during the harsh reaction conditions [67]. During the reaction process, soluble materials leached into the electrolyte, as confirmed by the nearly absent Cl 2p XPS spectra, leading to a balance of the alkaline-earth metal ion concentration between the host phase and the interfacial liquid. Benefitting from this unique leaching effect, the perovskite surface crystalline matrix was well preserved after the harsh oxidation conditions compared to that of the pure perovskite phase (Figure 4a,b). As a result, a perovskite with a well-preserved crystalline surface after the OER exhibited dramatically improved OER activity compared to that of the amorphous sample. Impressively, the hybrid catalyst requires a low overpotential of 260 mV to obtain a current density of 10 mA cm^{-2} , which is approximately 137 mV lower than that of the pure-phase material (Figure 4c). Notably, the OER activity of the hybrid catalyst represents the top level among recently reported perovskite oxide materials. Thus, the proposed design strategy can effectively change the reaction mechanism, allowing control of the surface reconstruction process (Figure 4d). In addition, the proposed methodology is a universal method that can also be applied to many types of oxides, such as single perovskites, double perovskites, and the Ruddlesden–Popper perovskite.

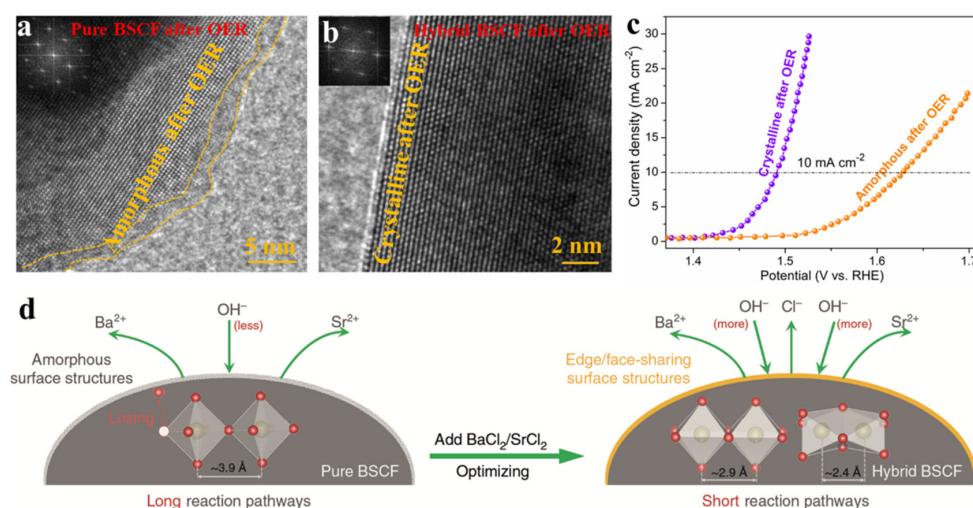


Figure 4. HRTEM images of the (a) pure-phase BSCF and (b) hybrid BSCF after OER tests. (c) LSV curves of the pure-phase BSCF and hybrid BSCF for the OER. (d) Schematic illustrations showing control of the surface change. Reproduced with permission [67]. Copyright 2020, Nature Publishing Group.

5. Accelerating Surface Reconstruction

5.1. Promoting Surface Reconstruction

The controllable leaching can promote the rate and level of surface reconstruction, which effectively increases the number of active sites on the catalyst surface. Moreover, the rate of anion/cation leaching is also dependent on the applied anodic potential. In this section, we briefly summarize the effects of cation and anion leaching for promoting surface reconstruction during the OER process.

Duan et al. reported controllable anodic leaching of Cr in a spinel oxide CoCr_2O_4 to obtain outstanding OER activity (Figure 5a) [113]. Remarkably, the higher the potential is applied the high concentration of Cr in the solution is detected (Figure 5b). In contrast, the level of Co leaching is independent of the applied potentials (Figure 5b). Moreover, the levels of Cr leaching are consistent with the increased electrocatalytic activities. First, the vacancies and defects induced by Cr leaching enable the formation of Co oxyhydroxide. Second, under higher anodic potentials, the further promoted Cr leaching and lattice oxygen consumption make reconstructed Co species with higher intrinsic activity per site (Figure 5c). Song's group reported cobalt oxychloride $\text{Co}_2(\text{OH})_3\text{Cl}$ that exhibited a gradual phase transition due to the etching of lattice Cl^- ions, alone with continuously increased OER activities [66]. The activated material shows an overpotential of 270 mV

at 10 mA cm^{-2} in an alkaline solution, which is comparable to that of noble metal oxide IrO_2 . The irreversible etching of the lattice Cl^- brought about numerous structural defects and high-valence Co species, which are demonstrated by aberration-corrected high-angle annular dark-field scanning transmission electron microscopy and operando synchrotron radiation-based X-ray spectroscopic characterizations, respectively (Figure 5d–f). Moreover, first-row transition metal sulfides, phosphides, and nitrides are also promising candidates for OER electrocatalysts in an alkaline environment. Of note, the surfaces of these materials are more prone to be oxidized to metal oxyhydroxide due to the fast surface reconstruction under the electrochemical oxidation condition [57,84,114]. Xu et al. evaluated the effect of the introduction of F into NiFe structure, which can enable a faster and deeper surface reconstruction process (Figure 5g) [114]. In detail, the precatalyst of NiFeO_xF_y nanosheets are easily changed into $\text{Ni(Fe)O}_x\text{H}_y$ compared with the initial NiFe precatalysts, which was demonstrated by operando Raman, ex-situ XPS spectra, and HRTEM analyses (Figure 5h,i). The positive effect of F-modification is also demonstrated in metal sulfide materials. For example, the surface of fluorinated Ni_3S_2 exhibits a low-crystalline nanosheet structure with obvious Ni-F bonds, which can greatly contribute to the formation of active NiOOH active species [115]. Additionally, the advantages of good conductivity and fast reaction kinetics of the fluorinated Ni_3S_2 catalyst jointly bring about the enhanced OER performance.

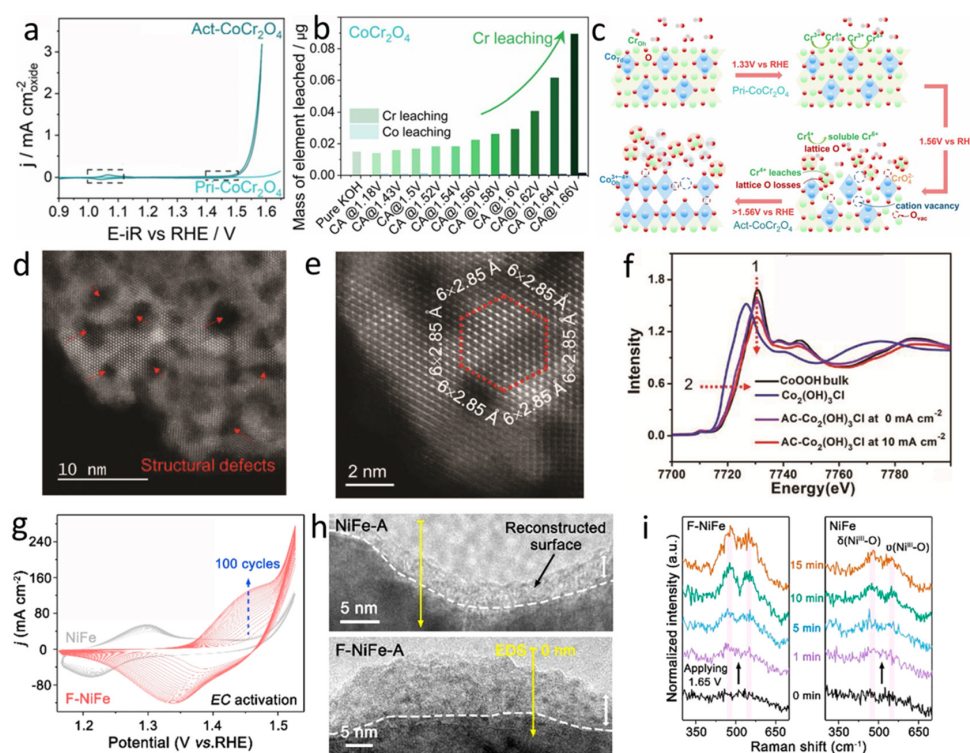


Figure 5. (a) CV curves of CoCr_2O_4 with the initial state (2nd cycle) and after chronoamperometry (at 1.7 V for 1.5 h). (b) The cumulative mass of Co and Cr leached after consecutive series of chronoamperometry conducted at 20 min interval for CoCr_2O_4 . (c) Scheme of CoCr_2O_4 surface reconstruction before OER testing after being applied increased potentials. Reproduced with permission [113]. Copyright 2021, Wiley-VCH. (d) STEM and (e) atomic-resolution HAADF-STEM images of the $\text{AC-Co}_2(\text{OH})_3\text{Cl}$. (f) Normalized Co K-edge XANES spectra of the $\text{Co}_2(\text{OH})_3\text{Cl}$, $\text{AC-Co}_2(\text{OH})_3\text{Cl}$ under OER and non-OER conditions as well as the reference (CoOOH bulk). Reproduced with permission [66]. Copyright 2019, Wiley-VCH. (g) CV curves of the F-NiFe and NiFe in an alkaline solution. (h) HRTEM images of F-NiFe-A and the NiFe-A. (i) Operando Raman spectra of F-NiFe and the NiFe. Reproduced with permission [114]. Copyright 2021, American Chemical Society.

5.2. Realizing Self-Terminated Surface Reconstruction

Inactive and low-cost materials as potential catalysts should be activated as high-performance OER electrocatalysts. In situ-generated active species (e.g., Co^{3+} oxyhydroxides) after surface reconstruction can serve as main active sites, offering high activity capabilities [55,62,86,116]. The challenge is how rationally and precisely to initiate the surface reconstruction of inactive catalysts. Furthermore, the restructuring degree should be kept under control. In many reported cases, bulk precatalysts serving as a template would be partly (or even completely) compromised to create a highly active surface. Therefore, the development of strategies for activating and terminating the surface reconstruction process is crucial.

Wu et al. reported Fe-doped CoAl_2O_4 to showcase this design strategy in the development of high-performance OER electrocatalysts based on inactive and low-cost spinel oxides [104]. After Fe substitution, a decrease in the number of Co valence states with the creation of oxygen vacancies and a raised O 2p level were observed for a $\text{CoFe}_{0.25}\text{Al}_{1.75}\text{O}_4$ sample, as confirmed by X-ray absorption near-edge structure (XANES) spectroscopy (Figure 6a,b). Modulation of the pre-oxidation states of Co^{2+} in $\text{CoFe}_{0.25}\text{Al}_{1.75}\text{O}_4$ provides a great potential for surface reconstruction to form surface-active species. In addition, an irreversible surface change with the generation of surface oxyhydroxide was demonstrated by the electrochemical behavior, with negligible changes of the pseudocapacitive charge after the second cyclic voltammetry (CV) cycle. For perovskite oxides, if lattice oxygen participates in the reaction, a descriptor of the O 2p level relative to the Fermi level can be involved during the reaction process. However, with regard to $\text{CoFe}_{0.25}\text{Al}_{1.75}\text{O}_4$, a ≈ 5 nm reconstructed surface was found after the first cycle, remaining quite stable during subsequent cycling (Figure 6c) and revealing the unlikely involvement of lattice oxygen during the reconstruction process. That is to say, surface reconstruction was triggered by lattice oxygen oxidation and could be quickly terminated after the first cycle. The reconstruction process was closely related to the leaching of metal cations, especially for the Al metal ions. The leaching of Al cations was found to be quite remarkable compared to that of Co and Fe cations. Importantly, Al leaching would end quickly, revealing a stable concentration of Al in the tested electrolytes stemming from the initial reaction process (Figure 6d). Furthermore, DFT calculations revealed that the energy of the O 2p level decreased when Al vacancies were introduced into the lattice (Figure 6e). Similar to the $\text{W}_{0.2}\text{Er}_{0.1}\text{Ru}_{0.7}\text{O}_{2-\delta}$ case, the lattice oxygen oxidation would end when the energy of the O 2p level was low. Thus, the reconstruction process stopped as no additional oxygen vacancies were created. Benefitting from the above-mentioned advantages, the cost-effective $\text{CoFe}_{0.25}\text{Al}_{1.75}\text{O}_4$ catalyst exhibited superior mass activity compared to that of the noble-metal oxide IrO_2 and benchmark transition-metal oxides (e.g., BSCF and $\text{Pr}_{0.5}\text{Ba}_{0.5}\text{CoO}_{3-\delta}$).

The proposed surface reconstruction self-terminated methodology can also be applied to other types of materials. Very recently, Wang et al. redirected the dynamic surface restructuring of layered transition-metal oxides [73]. From the DFT-calculated reaction energy profile, delithiation is energetically unfavorable for the LiCoO_2 oxide and requires a higher potential level to trigger surface reconstruction to $\text{Li}_{1\pm x}\text{Co}_2\text{O}_4$ and longer cycles for stabilization (Figure 6f). Cl-doping can reduce the electrochemical potential to initiate cobalt oxidation and lithium leaching, causing to the surface to transform into a self-terminated amorphous (oxy)hydroxide (Figure 6g). The operando XAFS spectra at the Co K-edge were collected to uncover the role of doped-Cl (Figure 6h). A decrease in the initial Co valence state of $\text{LiCoO}_{1.8}\text{Cl}_{0.2}$ leads to a greater increase in the Co valence than that in LiCoO_2 within the same anodic potential range (Figure 6i). Notably, the restructuring process for $\text{LiCoO}_{1.8}\text{Cl}_{0.2}$ is completely irreversible, as demonstrated by the negligible change of the XANES outcomes after 20 CV cycles. In contrast, for the cycled sample of LiCoO_2 , the corresponding Co K-edge shifted further during the electrochemical reaction (Figure 6j), indicating that either the restructuring process was not complete or that the reconstructed phase was unstable. Moreover, transition-metal oxyhydroxides are reportedly more active than their spinel counterparts. The OER activity of surface-restructured

LiCoO_{1.8}Cl_{0.2} outperformed many state-of-the-art OER catalysts. By manipulating the in situ catalyst leaching, this work deepens our understanding of modulated surface restructuring (Figure 6k).

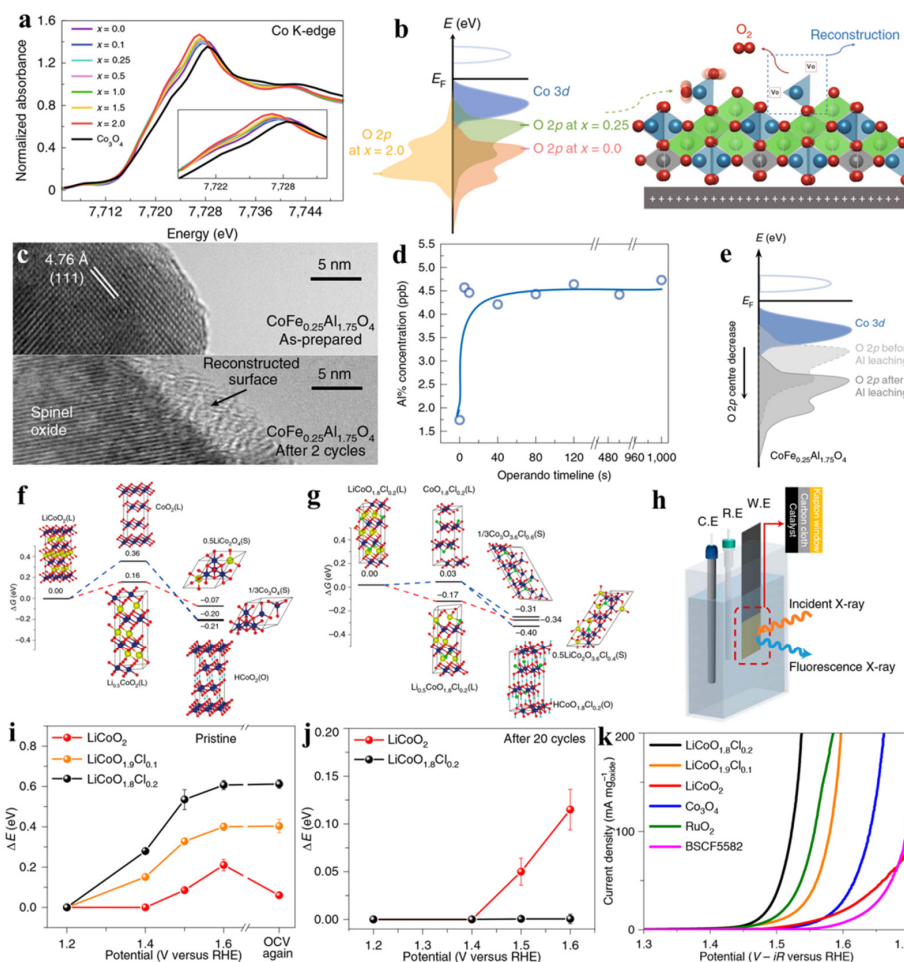


Figure 6. (a) Co K-edge XANES spectra of Fe-doped CoAl₂O₄ samples. (b) Schematic band illustrations of CoAl₂O₄, CoFe_{0.25}Al_{1.75}O₄, and CoFe₂O₄, and schematic demonstration of the surface reconstruction of CoFe_{0.25}Al_{1.75}O₄. (c) HRTEM images of the CoFe_{0.25}Al_{1.75}O₄ catalyst before and after OER tests. (d) Al concentration in the reaction electrolyte during the OER process. (e) Comparison of the band structure of CoFe_{0.25}Al_{1.75}O₄ with and without Al³⁺ vacancies. Reproduced with permission [104]. Copyright 2019, Nature Publishing Group. Reaction energy profiles at 1.6 V versus RHE for (f) LiCoO₂ and (g) LiCoO_{1.8}Cl_{0.2}. (h) Experimental set-up scheme for operando testing. (i) Co K-edge shift at different potentials for fresh samples. (j) Co K-edge shift for cycled samples. (k) OER mass activity for LiCoO₂, LiCoO_{1.9}Cl_{0.1}, LiCoO_{1.8}Cl_{0.2}, Co₃O₄, BSCF, and RuO₂. Reproduced with permission [73]. Copyright 2021, Nature Publishing Group.

5.3. Realizing Deep Reconstruction

Independent of material types and particle sizes, for most reported OER-precatalysts, the values of reconstruction layer thickness are less than 10 nm [85]. Considering the highly active of in situ formed metal oxyhydroxides, it is reasonable to expect that the electrochemical performance of precatalysts would be greatly improved with the enhanced surface reconstruction level, namely deep surface reconstruction [117,118]. Limited by the characteristic of the electrochemical process (the catalysis takes place on the surface of catalysts) and catalyst structures (e.g., particle size and morphology), it is still changing to realize the deep reconstruction and the related universal design methods are strongly demanded.

Wang et al. reported that a rapid and deep self-reconstruction of precatalysts could be realized by an anion etching process (Figure 7a) [119]. The precatalyst is made of a core-shell structure, where NiMoO_4 is the core and $\text{NiFe}/\text{Ni-FeO}_x$ nanoparticles in N-doped amorphous carbon is the shell. The fast dissolution rate of MoO_4^{2-} and incorporation of Fe in the Ni-oxyhydroxide leads to the in situ generation of $\text{NiFeOOH}/\text{NiFe LDH}$ (Figure 7b–e), which contributes to the rapid and deep self-reconstruction process. Yan et al. utilized the advantage of hollow structure to promote the reconstruction level (Figure 7f) [118]. In particular, the in situ Raman spectroscopy confirmed the positive effect of hollow structure on facilitating the deep reconstruction (Figure 7g,h). In detail, the precatalyst of $\text{Ni}_5\text{P}_2/\text{FeP}_4$ nanoboxes deeply reconstruct into $\text{NiOOH}/\text{FeOOH}$ nanosheet (Figure 7i). Moreover, the considerable interface between FeOOH and NiOOH and abundant defects jointly contribute to superior OER activity (Figure 7j).

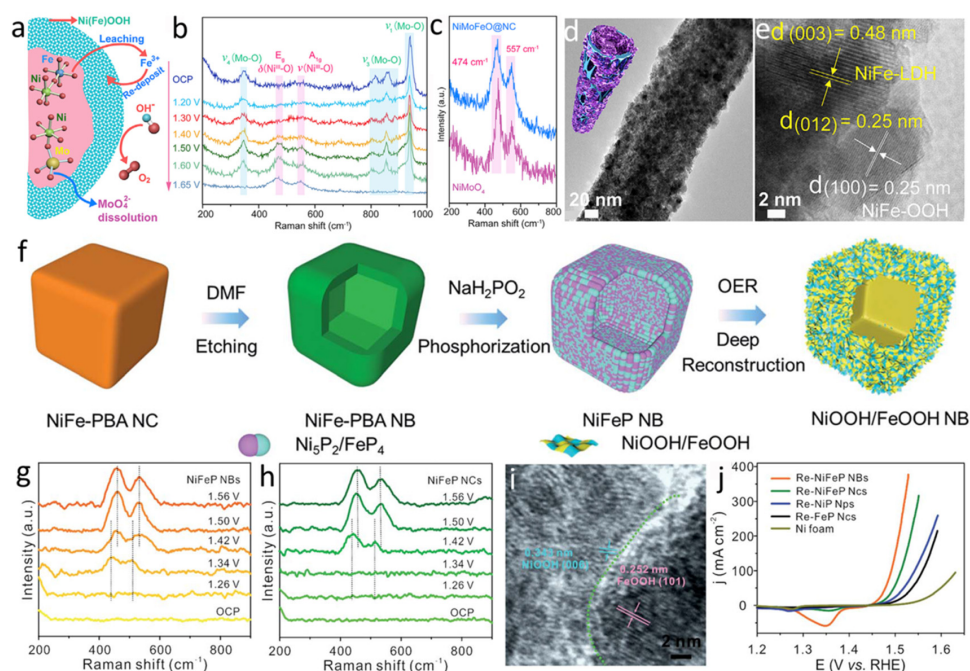


Figure 7. (a) Schematic of the reconstruction process for NiMoFeO@NC . (b) Operando Raman spectra of NiMoFeO@NC . (c) Operando Raman spectra of NiMoFeO@NC and NiMoO_4 obtained at 1.65 V. (d) Low-magnification and (e) high-magnification TEM images of NiMoFeO@NC after electrochemical reaction. Reproduced with permission [119]. Copyright 2020, Cell Press. (f) Schematic for the formation of precatalysts and deep reconstruction process of precatalysts into hierarchical $\text{NiOOH}/\text{FeOOH}$ structures. Operando Raman spectra of (g) NiFeP NBs and (h) NiFeP NCs at different applied potentials. (i) HRTEM image of $\text{NiOOH}/\text{FeOOH}$ structures. (j) LSV curves of catalysts loaded on Ni foam after 30 h of reconstruction process. Reproduced with permission [118]. Copyright 2021, Royal Society of Chemistry.

6. Making Complete Reconstruction

For surface reconstruction and deep reconstruction, the in situ formed layer would lead to a core-shell structure, where the in situ-formed active species and the unchanged precatalyst serve as the shell and core, respectively [14,63,75,92,104,120–122]. When the core material cannot favorably contribute to the shell or when the core material has the potential to be transformed further into active species, traditional near-surface reconstruction would have considerable limitations [85]. Complete changes of bulk materials can enhance the active sites to a great extent, but this remains a major challenge [85,123].

Very recently, Liu and his-worker demonstrated a complete-change mechanism [85]. The key factor to induce complete reconstruction is to construct a loose surface layer. For the NiMoO_4 catalyst, a low degree of surface reconstruction was found due to a dense

restructured layer, leading to a core-shell $\text{NiMoO}_4@\text{NiOOH}$ structure. The strategy of etching–leaching engineering was presented to realize the complete reconstruction effect in a bulk hydrate precatalysts system. Specifically, for the rational designed precatalyst of $\text{NiMoO}_4 \cdot x\text{H}_2\text{O}$, the co-leaching of soluble Mo species and crystal water during the OER process in an alkaline solution created a considerable nanoporous structure with the generation of high-valence Ni^{3+} species (NiOOH). Finally, the generated nanoporous and loose layer played a crucial role in triggering the full diffusion of electrolytes into the inner structures, by which the goal of a complete change was achieved (Figure 8a). The surface change process involved microstructures of intermediates, as was visually revealed in ex situ HRTEM images (Figure 8b). The process consisted of an amorphous surface at an ultralow overpotential, an additional change at a high overpotential (including NiOOH , amorphous area, and $\text{NiMoO}_4 \cdot x\text{H}_2\text{O}$), and complete reconstruction. The potential-dependent in situ Raman spectra further demonstrated the reaction mechanism. Bond breakage, a co-leaching effect, and active species generation could be confirmed by the disappearance of peaks (at $\approx 355 \text{ cm}^{-1}$ corresponding to MoO_4 vibration and at ≈ 820 and 950 cm^{-1} corresponding to Mo-O-Ni stretching in $\text{NiMoO}_4 \cdot x\text{H}_2\text{O}$) and the generation of new peaks with relatively high intensity levels (at 474 and 554 cm^{-1} corresponding to the Ni-O vibration of NiOOH and 900 cm^{-1} corresponding to MoO_4^{2-} in an alkaline solution) (Figure 8c). The superior electrocatalytic activities of the completely reconstructed catalyst were demonstrated by LSV curves normalized to a geometric area (Figure 8d) and an electrochemically active surface area (Figure 8e). The completely reconstructed catalyst (NiOOH) exhibited clearly enhanced activity compared to the surface-reconstructed catalyst ($\text{NiMoO}_4@\text{NiOOH}$ with a core-shell structure) and a commercial noble-metal-based Ir/C catalyst. More importantly, a negligible change of the potential during the 1350 h stability test according to chronopotentiometric measurements was observed for the completely reconstructed catalyst, suggesting vast superiority of the in situ-formed microstructure by the complete reconstruction and also excellent potential as a cost-effective alternative to noble-metal oxides (Figure 8f).

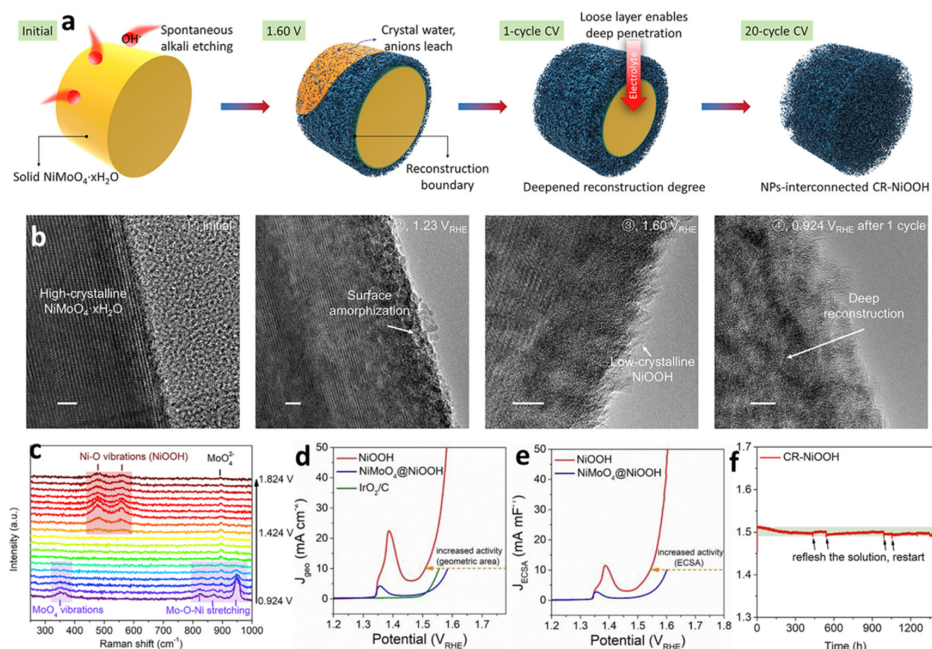


Figure 8. (a) Schematic diagrams of the complete surface change process for $\text{NiMoO}_4 \cdot x\text{H}_2\text{O}$. (b) Ex situ HRTEM images of the different reconstruction degrees at various activated stages of $\text{NiMoO}_4 \cdot x\text{H}_2\text{O}$. Scale bars, 5 nm. (c) In situ Raman spectra of $\text{NiMoO}_4 \cdot x\text{H}_2\text{O}$ during the OER process. LSV curves of the studied catalysts for the OER normalized by the (d) geometric area and (e) electrochemically active surface area. (f) Ultra-long stability test of the completely reconstructed NiOOH at a current density of 10 mA cm^{-2} . Reproduced with permission [85]. Copyright 2020, Cell Press.

7. Conclusions and Outlooks

Rational control of the surface reconstruction process is an effective strategy to develop high-performance OER electrocatalysts (Table 1). This calls for the overall consideration of rationally design precatalysts, an in-depth understanding of the surface reconstruction mechanism, and the exploration of effective design strategies (Figure 1). In this review, recent progress and design strategies related to this topic are summarized for advanced OER electrocatalysts. Beyond these processes to date, there remain many challenges and opportunities for those involved in the design of next-generation catalysts.

Table 1. Summary of OER performance of discussed catalysts in the main text.

Catalysts	Reconstruction Strategies	Overpotential (mV)	Tafel Slope (mV dec ⁻¹)	Stability	Ref.
W _{0.2} Er _{0.1} Ru _{0.7} O _{2-δ}	Limiting surface reconstruction	168 @ η10	66.8	η10 @ 500 h	[102]
hybrid BSCF	Maintaining surface crystalline matrix	260 @ η10	N.A.	10 mA @ 100 h	[67]
Co ₂ (OH) ₃ Cl	Promoting surface reconstruction	270 @ η10	155	η10 @ 10 h	[66]
NiFeO _x F _y	Promoting surface reconstruction	218 @ η10	31	η10-200 @ 50 h	[114]
NiFe-OH-F-SR	Promoting surface reconstruction	228 @ η100	22.6	η50 @ 60 h	[66]
F-Ni ₃ S ₂	Promoting surface reconstruction	239 @ η10	36	η50 @ 24 h	[115]
CoFe _{0.25} Al _{1.75} O ₄	Self-terminated surface reconstruction	~270 @ η~3.5	N.A.	η~3.5 @ 48 h	[104]
LiCoO _{1.8} Cl _{0.2}	Self-terminated surface reconstruction	270 @ η10	55.4	η20 @ 500 h	[73]
Self-Reconcat					
NiMoFeO@NC	Deep reconstruction	270 @ η50	66.6	η100 @ 24 h	[119]
Ni ₅ P ₂ /FeP ₄	Deep reconstruction	246 @ η10	41	η50 @ 50 h	[118]
NiMoO ₄ ·xH ₂ O nanowires	Complete reconstruction	278.2 @ η10	N.A.	η10 @ 1350 h	[85]

7.1. Rational Design of Precatalysts

7.1.1. Design Precatalysts

The most widely reported active layers after surface reconstruction are oxyhydroxides [62]. Thus, the relationship between the restructuring behavior and the observed electrocatalytic activity is a significant research topic for those involved in the design of OER catalysts. Additionally, for most catalysts after surface-structure self-reconstruction, a core-shell structure is formed. The in situ generated active layer and the remaining precatalyst act as the shell and the core, respectively [24,87]. Thus, the requirements of the core located between the current collector and the shell structure are also critical.

7.1.2. Reaction Mechanisms

Though in situ-formed species during structural self-reconstruction work as active sites for the OER, the reconstruction mechanism is closely related to the physicochemical properties of the precatalysts used. For example, unlike the conventionally reported irreversible surface change, Bergmann found the structurally reversible change of the crystalline Co₃O₄ catalyst [124]. In contrast to the crystalline Co₃O₄ catalyst, when an oxygen vacancy was introduced into Co₃O₄, the oxygen vacancy could initialize the surface reconstruction process at a relatively low potential, even before the occurrence of the OER process, compared with that of the pure spinel Co₃O₄ catalyst [125]. Therefore, rational design of the precatalyst is the key factor determining the electrocatalytic activities and reaction mechanism. Exploring innovative strategies to design high-performance electrocatalysts is of great importance. In addition, if the proposed design strategy is universal, it can guide the design of more advanced electrocatalysts.

7.1.3. New Catalyst Design Concepts

The dissolution of metals (e.g., alkaline and alkaline earth elements) into electrolytes to induce surface reconstruction is widely reported in relation to the design of high-performance electrocatalysts [14,89,110,126–128]. The observed electrocatalytic process is highly dependent on the dissolution rate and the final surface species, which form; this

is also related to the applied potential and time under an anodic condition [84,128,129]. Thus, the continuous dissolution may be a drawback in terms of long-term application. For example, currently reported OER materials can only work a few hours at a low current density (e.g., 10 mA cm^{-2} is typically used) [130,131]. For practical applications, a high current density, high potential, and high gas production rate are often involved; the shedding and dissolution of the catalysts are tough problems to solve [23,130,132,133]. To avoid these intractable issues, very recently the Cao group proposed a novel concept similar to homogeneous catalysis to fabricate in situ regenerative electrodes that could exhibit high OER activity and superior long-time stability level when operated at a high current density [129]. Specifically, precatalysts were demonstrated as the Co and Fe bimetal salt solutions, which were mixed with an alkaline solution before the reaction. Notably, a conventional three-electrode set-up was used, with bare carbon paper acting as the working electrode initially. During the electrochemical process, homogeneous Co and Fe ions in the electrolyte were consumed and in situ transformed into active species on the surface of the carbon paper at the applied OER potentials. As indicated by the OER curves, the OER activities were gradually enhanced with an increase in the number of CV cycles, which was also confirmed according to the increased active species tested by the electrochemically active surface area. The in situ generation process of active sites could reach a steady state, as reflected by the unchanged activity after 400 CV cycles. Systematical characterizations were conducted to study changes of the active species after they were formed on the surface of the carbon paper. These results showed that the initial CoFe hydroxides would be in situ transformed into CoFe oxyhydroxide on the substrate surface during the oxidation process. Moreover, in contrast to ex situ techniques, in situ XANES provides fine-grained information about the electronic and geometric structures. For example, the in situ Co XANES result demonstrated that Co^{3+} ions could further be oxidized to Co^{4+} ions, as confirmed by a positive energy shift and a shorter Co-O bond compared with that of the ex situ Co XANES. This work provides a novel strategy to design highly active and stability electrodes.

7.2. In-Depth Understanding of Reconstruction Mechanisms

Depending on the types of materials used (e.g., spinel oxide, perovskite oxide, layered oxide and metal oxide-based composites) and the different physicochemical properties of the precatalysts, the actual surface reconstruction mechanism can differ [9,63,79,97]. For example, the surface structure of the perovskite oxide LaCoO_3 was reported to be quite stable under cycling conditions [62,69,134]. Based on the available literature, stable OER performance under continuous cycling demonstrate there is likely no or negligible surface changes. Regarding the above-mentioned $\text{CoFe}_{0.25}\text{Al}_{1.75}\text{O}_4$ catalyst, there was a quick self-termination process during the OER, [104] while the thickness of the reconstructed surface layers depends strongly on the number of OER cycles for most reported catalysts (e.g., $\text{La}_2\text{CoMnO}_6$ and SrIrO_3 thin films) [60,103]. Furthermore, Zhou et al. reported another reconstruction mechanism by which the valence state of a transition metal (Co) under OER conditions was highly dependent on the applied voltage and reaction times, whereas the spin state of Co ions and the edge-sharing Co-O network remained unchanged [93]. Therefore, to gain a deeper understanding of the reaction mechanisms for these types of designed catalysts, comprehensive studies are needed. More importantly, recently developed descriptors to predict the electrochemical activity level of designed catalysts are generally based on the physicochemical properties of the precatalysts without consideration of dynamic changes during the electrochemical reaction [49,135–137]. Therefore, developing activity descriptors based on the physicochemical properties of precatalysts and on the surface reconstruction process remains a challenging task that is also urgently needed.

7.3. In Situ/Operando Techniques

Generally, it is difficult to capture intermediates with a short lifetime, or to observe dynamic changes by ex situ characterization approaches. To track the surface change dur-

ing an electrochemical reaction, in situ/operando techniques, specifically in situ/operando XRD/XPS/TEM/XAS/Raman methods, are the most powerful tools [61,63,82,94,138,139]. For example, in situ XAS can provide informative data regarding dynamic changes of the valence state, coordination number, and bond length [72,81,94,140]. Meanwhile, the in situ/operando Raman technique is sensitive to structural changes at different stages under a wide range of electrochemical reaction conditions [72,82,97,141]. It is important to note that it is also difficult to obtain an in-depth understanding of the reconstruction mechanism by only a single in situ/operando technique because each technique has a distinct role due to its application scope [82]. Thus, to reveal precisely the reaction mechanism pertaining to surface reconstruction, a combination of various techniques is needed [63,67,142]. For example, a representative work by Chen's group utilized three in situ techniques to unravel the real-time changes of a state-of-the-art bifunctional catalyst [143]. Specifically, to determine the dynamic changes that affect the morphology, interface state, and chemical state, in situ TEM, in situ Raman, and in situ XAS were utilized, respectively.

7.4. Bridging the Gap between Fundamental Designs and Practical Applications

Considerable efforts have been devoted toward designing high-performance electrocatalysts in fundamental research. Typically, activity evaluations on the laboratory scale are conducted at room temperature [10]. However, there may be a gap between fundamental designs and practical applications. For example, the industrial process of alkaline water electrolysis is operated at 50–80 °C in a high concentration of electrolyte (≈ 30 wt.% KOH) [56,85,144]. Differences in the surface reconstruction mechanisms between room temperature and industrial temperatures were studied by Liu et al [56]. A thermally induced complete reconstruction phenomenon was found, which is much different from that of catalysts, which operate at room temperature. Therefore, proper control of the surface reconstruction process under practical application conditions is an ongoing issue.

Funding: This research was funded by the Hydrogen Energy Innovation Technology Development Program, grant number NRF-2019M3E6A1064523; Nano Material Technology Development Program, grant number 2017M3A7B4049547; National R&D Program through the National Research Foundation of Korea (NRF) funded by the Ministry of Science, ICT and Future Planning, grant number 2020M3H4A3105824; Basic project (referring to projects performed with the budget directly contributed by the Government to achieve the purposes of establishment of Government-funded research Institutes)" and funded by the KOREA RESEARCH INSTITUTE of CHEMICAL TECHNOLOGY (KRICT), grant number KS2122-10.

Institutional Review Board Statement: Not applicable.

Informed Consent Statement: Not applicable.

Data Availability Statement: Not applicable.

Conflicts of Interest: The authors declare no conflict of interest.

References

1. Seh, Z.W.; Kibsgaard, J.; Dickens, C.F.; Chorkendorff, I.; Norskov, J.K.; Jaramillo, T.F. Combining theory and experiment in electrocatalysis: Insights into materials design. *Science* **2017**, *355*, eaad4998. [[CrossRef](#)]
2. Gao, R.; Wang, J.; Huang, Z.-F.; Zhang, R.; Wang, W.; Pan, L.; Zhang, J.; Zhu, W.; Zhang, X.; Shi, C.; et al. Pt/Fe₂O₃ with Pt–Fe pair sites as a catalyst for oxygen reduction with ultralow Pt loading. *Nat. Energy* **2021**, *6*, 614–623. [[CrossRef](#)]
3. Kim, H.; Seo, H.G.; Choi, Y.; Lim, D.-K.; Jung, W. Cathodic electrochemical deposition: A new strategy to enhance the activity and stability of silver cathodes for thin-film solid oxide fuel cells. *J. Mater. Chem. A* **2020**, *8*, 14491–14497. [[CrossRef](#)]
4. Jo, S.; Sharma, B.; Park, D.H.; Myung, J.H. Materials and nano-structural processes for use in solid oxide fuel cells: A review. *J. Korean Ceram. Soc* **2020**, *57*, 135–151. [[CrossRef](#)]
5. Li, Y.; Sun, Y.; Qin, Y.; Zhang, W.; Wang, L.; Luo, M.; Yang, H.; Guo, S. Recent Advances on Water-Splitting Electrocatalysis Mediated by Noble-Metal-Based Nanostructured Materials. *Adv. Energy Mater.* **2020**, *10*, 1903120. [[CrossRef](#)]
6. Li, M.; Bi, X.; Wang, R.; Li, Y.; Jiang, G.; Li, L.; Zhong, C.; Chen, Z.; Lu, J. Relating Catalysis between Fuel Cell and Metal-Air Batteries. *Matter* **2020**, *2*, 32–49. [[CrossRef](#)]
7. Hu, C.; Zhang, L.; Gong, J. Recent progress made in the mechanism comprehension and design of electrocatalysts for alkaline water splitting. *Energy Environ. Sci.* **2019**, *12*, 2620–2645. [[CrossRef](#)]

8. Wang, K.; Sun, K.; Li, Z.; Lv, Z.; Yu, T.; Liu, X.; Wang, G.; Xie, G.; Jiang, L. Preparation of Fe–Co–P–Gr/NF Coating via Electroless Composite Plating as Efficient Electrocatalysts for Overall Water Splitting. *Electron. Mater. Lett.* **2020**, *16*, 164–173. [[CrossRef](#)]
9. Lei, Z.; Wang, T.; Zhao, B.; Cai, W.; Liu, Y.; Jiao, S.; Li, Q.; Cao, R.; Liu, M. Recent Progress in Electrocatalysts for Acidic Water Oxidation. *Adv. Energy Mater.* **2020**, *10*, 2000478. [[CrossRef](#)]
10. Wei, C.; Rao, R.R.; Peng, J.; Huang, B.; Stephens, I.E.L.; Risch, M.; Xu, Z.J.; Shao-Horn, Y. Recommended Practices and Benchmark Activity for Hydrogen and Oxygen Electrocatalysis in Water Splitting and Fuel Cells. *Adv. Mater.* **2019**, *31*, 1806296. [[CrossRef](#)] [[PubMed](#)]
11. Fei, L.; Sun, H.; Ran, R.; Zhou, W.; Shao, Z. Self-Supported Nickel Phosphide Electrode for Efficient Alkaline Water-to-Hydrogen Conversion via Urea Electrolysis. *Ind. Eng. Chem. Res.* **2021**, *60*, 1185–1193. [[CrossRef](#)]
12. Huang, Z.-F.; Xi, S.; Song, J.; Dou, S.; Li, X.; Du, Y.; Diao, C.; Xu, Z.J.; Wang, X. Tuning of lattice oxygen reactivity and scaling relation to construct better oxygen evolution electrocatalyst. *Nat. Commun.* **2021**, *12*, 3992. [[CrossRef](#)] [[PubMed](#)]
13. Li, Y.; Chen, G.; Zhu, Y.; Hu, Z.; Chan, T.-S.; She, S.; Dai, J.; Zhou, W.; Shao, Z. Activating Both Basal Plane and Edge Sites of Layered Cobalt Oxides for Boosted Water Oxidation. *Adv. Funct. Mater.* **2021**, 2103569. [[CrossRef](#)]
14. Seitz, L.C.; Dickens, C.F.; Nishio, K.; Hikita, Y.; Montoya, J.; Doyle, A.; Kirk, C.; Vojvodic, A.; Hwang, H.Y.; Norskov, J.K.; et al. A highly active and stable IrO_x/SrIrO_x catalyst for the oxygen evolution reaction. *Science* **2016**, *353*, 1011. [[CrossRef](#)] [[PubMed](#)]
15. Shan, J.; Guo, C.; Zhu, Y.; Chen, S.; Song, L.; Jaroniec, M.; Zheng, Y.; Qiao, S.-Z. Charge-Redistribution-Enhanced Nanocrystalline Ru@IrO_x Electrocatalysts for Oxygen Evolution in Acidic Media. *Chem* **2019**, *5*, 445–459. [[CrossRef](#)]
16. Chao, T.; Hu, Y.; Hong, X.; Li, Y. Design of Noble Metal Electrocatalysts on an Atomic Level. *ChemElectroChem* **2019**, *6*, 289–303. [[CrossRef](#)]
17. An, L.; Wei, C.; Lu, M.; Liu, H.; Chen, Y.; Scherer, G.G.; Fisher, A.C.; Xi, P.; Xu, Z.J.; Yan, C.-H. Recent Development of Oxygen Evolution Electrocatalysts in Acidic Environment. *Adv. Mater.* **2021**, *33*, 2006328. [[CrossRef](#)] [[PubMed](#)]
18. Li, L.; Wang, P.; Shao, Q.; Huang, X. Recent Progress in Advanced Electrocatalyst Design for Acidic Oxygen Evolution Reaction. *Adv. Mater.* **2021**, 2004243. [[CrossRef](#)]
19. Cai, W.; Yang, H.; Zhang, J.; Chen, H.-C.; Tao, H.B.; Gao, J.; Liu, S.; Liu, W.; Li, X.; Liu, B. Amorphous Multimetal Alloy Oxygen Evolving Catalysts. *ACS Mater. Lett.* **2020**, *2*, 624–632. [[CrossRef](#)]
20. Wang, C.; Jin, L.; Shang, H.; Xu, H.; Shiraishi, Y.; Du, Y. Advances in engineering RuO₂ electrocatalysts towards oxygen evolution reaction. *Chin. Chem. Lett.* **2021**, *32*, 2108–2116. [[CrossRef](#)]
21. Sun, H.; Jung, W. Recent Advances in Doped Ruthenium Oxides as High-Efficiency Electrocatalysts for Oxygen Evolution Reaction. *J. Mater. Chem. A* **2021**, *9*, 15506–15521. [[CrossRef](#)]
22. Zhang, L.; Jang, H.; Liu, H.; Kim, M.G.; Yang, D.; Liu, S.; Liu, X.; Cho, J. Sodium-Decorated Amorphous/Crystalline RuO₂ with Rich Oxygen Vacancies: A Robust pH-Universal Oxygen Evolution Electrocatalyst. *Angew. Chem. Int. Ed.* **2021**, *60*, 18821–18829. [[CrossRef](#)] [[PubMed](#)]
23. Zeng, K.; Zheng, X.; Li, C.; Yan, J.; Tian, J.-H.; Jin, C.; Strasser, P.; Yang, R. Recent Advances in Non-Noble Bifunctional Oxygen Electrocatalysts toward Large-Scale Production. *Adv. Funct. Mater.* **2020**, *30*, 2000503. [[CrossRef](#)]
24. Zhang, J.; Gao, M.; Luo, J.-L. In-situ Exsolved Metal Nanoparticles: A Smart Approach for Optimization of Catalysts. *Chem. Mater.* **2020**, *32*, 5424–5441. [[CrossRef](#)]
25. Zhang, Y.; Lin, Y.; Duan, T.; Song, L. Interfacial engineering of heterogeneous catalysts for electrocatalysis. *Mater. Today* **2021**, in press. [[CrossRef](#)]
26. Sun, H.; Xu, X.; Song, Y.; Zhou, W.; Shao, Z. Designing High-Valence Metal Sites for Electrochemical Water Splitting. *Adv. Funct. Mater.* **2021**, *31*, 2009779. [[CrossRef](#)]
27. Wang, J.; Kim, J.; Choi, S.; Wang, H.; Lim, J. A Review of Carbon-Supported Nonprecious Metals as Energy-Related Electrocatalysts. *Small Methods* **2020**, *4*, 2000621. [[CrossRef](#)]
28. Wang, J.; Kong, H.; Zhang, J.; Hao, Y.; Ciucci, F.J.Pi.M.S. Carbon-based Electrocatalysts for Sustainable Energy Applications. *Prog. Mater. Sci.* **2020**, *116*, 100717. [[CrossRef](#)]
29. Sun, H.; Song, S.; Xu, X.; Dai, J.; Yu, J.; Zhou, W.; Shao, Z.; Jung, W. Recent Progress on Structurally Ordered Materials for Electrocatalysis. *Adv. Energy Mater.* **2021**, 2101937. [[CrossRef](#)]
30. Zhao, D.; Lu, Y.; Ma, D. Effects of Structure and Constituent of Prussian Blue Analogs on Their Application in Oxygen Evolution Reaction. *Molecules* **2020**, *25*, 2304. [[CrossRef](#)]
31. Dou, S.; Wang, X.; Wang, S. Rational Design of Transition Metal-Based Materials for Highly Efficient Electrocatalysis. *Small Methods* **2019**, *3*, 1800211. [[CrossRef](#)]
32. Hu, Q.; Li, G.; Han, Z.; Wang, Z.; Huang, X.; Yang, H.; Zhang, Q.; Liu, J.; He, C. Recent progress in the hybrids of transition metals/carbon for electrochemical water splitting. *J. Mater. Chem. A* **2019**, *7*, 14380–14390. [[CrossRef](#)]
33. Wang, H.; Zhou, M.; Choudhury, P.; Luo, H. Perovskite oxides as bifunctional oxygen electrocatalysts for oxygen evolution/reduction reactions—A mini review. *Appl. Mater. Today* **2019**, *16*, 56–71. [[CrossRef](#)]
34. Feng, C.; Faheem, M.B.; Fu, J.; Xiao, Y.; Li, C.; Li, Y. Fe-Based Electrocatalysts for Oxygen Evolution Reaction: Progress and Perspectives. *ACS Catal.* **2020**, *10*, 4019–4047. [[CrossRef](#)]
35. Sun, H.; Xu, X.; Hu, Z.; Tjeng, L.H.; Zhao, J.; Zhang, Q.; Lin, H.-J.; Chen, C.-T.; Chan, T.-S.; Zhou, W.; et al. Boosting the oxygen evolution reaction activity of a perovskite through introducing multi-element synergy and building an ordered structure. *J. Mater. Chem. A* **2019**, *7*, 9924–9932. [[CrossRef](#)]

36. Sun, H.; He, J.; Hu, Z.; Chen, C.-T.; Zhou, W.; Shao, Z. Multi-active sites derived from a single/double perovskite hybrid for highly efficient water oxidation. *Electrochim. Acta* **2019**, *299*, 926–932. [[CrossRef](#)]
37. Sun, H.; Hu, Z.; Xu, X.; He, J.; Dai, J.; Lin, H.-J.; Chan, T.-S.; Chen, C.-T.; Tjeng, L.H.; Zhou, W.; et al. Ternary Phase Diagram-Facilitated Rapid Screening of Double Perovskites As Electrocatalysts for the Oxygen Evolution Reaction. *Chem. Mater.* **2019**, *31*, 5919–5926. [[CrossRef](#)]
38. Xu, X.; Pan, Y.; Ge, L.; Chen, Y.; Mao, X.; Guan, D.; Li, M.; Zhong, Y.; Hu, Z.; Peterson, V.K.; et al. High-Performance Perovskite Composite Electrocatalysts Enabled by Controllable Interface Engineering. *Small* **2021**, *17*, 2101573. [[CrossRef](#)]
39. Xu, X.; Pan, Y.; Zhong, Y.; Ran, R.; Shao, Z. Ruddlesden–Popper perovskites in electrocatalysis. *Mater. Horiz.* **2020**, *7*, 2519–2565. [[CrossRef](#)]
40. Ma, N.; Chen, G.; Zhu, Y.; Sun, H.; Dai, J.; Chu, H.; Ran, R.; Zhou, W.; Cai, R.; Shao, Z. A Self-Assembled Hetero-Structured Inverse-Spinel and Anti-Perovskite Nanocomposite for Ultrafast Water Oxidation. *Small* **2020**, *16*, 2002089. [[CrossRef](#)]
41. Chu, S.; Sun, H.; Chen, G.; Chen, Y.; Zhou, W.; Shao, Z. Rationally designed Water-Insertable Layered Oxides with Synergistic Effect of Transition-Metal Elements for High-Performance Oxygen Evolution Reaction. *ACS Appl. Mater. Interfaces* **2019**, *11*, 25227–25235. [[CrossRef](#)] [[PubMed](#)]
42. Zhang, A.; Liang, Y.; Zhang, H.; Geng, Z.; Zeng, J. Doping regulation in transition metal compounds for electrocatalysis. *Chem. Soc. Rev.* **2021**, *50*, 9817–9844. [[CrossRef](#)] [[PubMed](#)]
43. Yi, H.; Liu, S.; Lai, C.; Zeng, G.; Li, M.; Liu, X.; Li, B.; Huo, X.; Qin, L.; Li, L.; et al. Recent Advance of Transition-Metal-Based Layered Double Hydroxide Nanosheets: Synthesis, Properties, Modification, and Electrocatalytic Applications. *Adv. Energy Mater.* **2021**, *11*, 2002863. [[CrossRef](#)]
44. Chen, G.; Zhu, Y.; Chen, H.M.; Hu, Z.; Hung, S.F.; Ma, N.; Dai, J.; Lin, H.J.; Chen, C.T.; Zhou, W.; et al. An Amorphous Nickel–Iron-Based Electrocatalyst with Unusual Local Structures for Ultrafast Oxygen Evolution Reaction. *Adv. Mater.* **2019**, *31*, 1900883. [[CrossRef](#)] [[PubMed](#)]
45. Chen, G.; Hu, Z.; Zhu, Y.; Gu, B.; Zhong, Y.; Lin, H.-J.; Chen, C.-T.; Zhou, W.; Shao, Z. A Universal Strategy to Design Superior Water-Splitting Electrocatalysts Based on Fast In Situ Reconstruction of Amorphous Nanofilm Precursors. *Adv. Mater.* **2018**, *30*, 1804333. [[CrossRef](#)]
46. Wang, J.; Gao, Y.; Kong, H.; Kim, J.; Choi, S.; Ciucci, F.; Hao, Y.; Yang, S.; Shao, Z.; Lim, J. Non-precious-metal catalysts for alkaline water electrolysis: Operando characterizations, theoretical calculations, and recent advances. *Chem. Soc. Rev.* **2020**, *49*, 9154–9196. [[CrossRef](#)] [[PubMed](#)]
47. Huang, Z.-F.; Song, J.; Dou, S.; Li, X.; Wang, J.; Wang, X. Strategies to Break the Scaling Relation toward Enhanced Oxygen Electrocatalysis. *Matter* **2019**, *1*, 1494–1518. [[CrossRef](#)]
48. Zhou, T.; Zhang, N.; Wu, C.; Xie, Y. Surface/interface nanoengineering for rechargeable Zn–air batteries. *Energy Environ. Sci.* **2020**, *13*, 1132–1153. [[CrossRef](#)]
49. Liu, J.; Liu, H.; Chen, H.; Du, X.; Zhang, B.; Hong, Z.; Sun, S.; Wang, W. Progress and Challenges Toward the Rational Design of Oxygen Electrocatalysts Based on a Descriptor Approach. *Adv. Sci.* **2020**, *7*, 1901614. [[CrossRef](#)]
50. Sun, H.; Dai, J.; Zhou, W.; Shao, Z. Emerging Strategies for Developing High-Performance Perovskite-Based Materials for Electrochemical Water Splitting. *Energy Fuels* **2020**, *34*, 10547–10567. [[CrossRef](#)]
51. Gao, L.; Cui, X.; Sewell, C.D.; Li, J.; Lin, Z. Recent advances in activating surface reconstruction for the high-efficiency oxygen evolution reaction. *Chem. Soc. Rev.* **2021**, *50*, 8428–8469. [[CrossRef](#)]
52. Xu, X.; Wang, W.; Zhou, W.; Shao, Z. Recent Advances in Novel Nanostructuring Methods of Perovskite Electrocatalysts for Energy-Related Applications. *Small Methods* **2018**, *2*, 1800071. [[CrossRef](#)]
53. Zhao, G.; Li, P.; Cheng, N.; Dou, S.X.; Sun, W. An Ir/Ni(OH)₂ Heterostructured Electrocatalyst for the Oxygen Evolution Reaction: Breaking the Scaling Relation, Stabilizing Iridium (V), and Beyond. *Adv. Mater.* **2020**, *32*, 2000872. [[CrossRef](#)] [[PubMed](#)]
54. Zhai, L.; Benedict Lo, T.W.; Xu, Z.-L.; Potter, J.; Mo, J.; Guo, X.; Tang, C.C.; Edman Tsang, S.C.; Lau, S.P. In Situ Phase Transformation on Nickel-Based Selenides for Enhanced Hydrogen Evolution Reaction in Alkaline Medium. *ACS Energy Lett.* **2020**, *5*, 2483–2491. [[CrossRef](#)]
55. Fabbri, E.; Nachttegaal, M.; Binninger, T.; Cheng, X.; Kim, B.-J.; Durst, J.; Bozza, F.; Graule, T.; Schäublin, R.; Wiles, L.; et al. Dynamic surface self-reconstruction is the key of highly active perovskite nano-electrocatalysts for water splitting. *Nat. Mater.* **2017**, *16*, 925–931. [[CrossRef](#)]
56. Liu, X.; Guo, R.; Ni, K.; Xia, F.; Niu, C.; Wen, B.; Meng, J.; Wu, P.; Wu, J.; Wu, X.; et al. Reconstruction-Determined Alkaline Water Electrolysis at Industrial Temperatures. *Adv. Mater.* **2020**, *32*, 2001136. [[CrossRef](#)]
57. Chen, J.; Chen, H.; Yu, T.; Li, R.; Wang, Y.; Shao, Z.; Song, S. Recent Advances in the Understanding of the Surface Reconstruction of Oxygen Evolution Electrocatalysts and Materials Development. *Electrochem. Energy Rev.* **2021**, *4*, 566–600. [[CrossRef](#)]
58. Cao, D.; Shou, H.; Chen, S.; Song, L. Manipulating and probing the structural self-optimization in oxygen evolution reaction catalysis. *Curr. Opin. Electrochem.* **2021**, *30*, 100788. [[CrossRef](#)]
59. Solomon, G.; Landström, A.; Mazzaro, R.; Jugovac, M.; Moras, P.; Cattaruzza, E.; Morandi, V.; Concina, I.; Vomiero, A. NiMoO₄@Co₃O₄ Core–Shell Nanorods: In Situ Catalyst Reconstruction toward High Efficiency Oxygen Evolution Reaction. *Adv. Energy Mater.* **2021**, *11*, 2101324. [[CrossRef](#)]
60. Song, C.W.; Suh, H.; Bak, J.; Bae, H.B.; Chung, S.-Y. Dissolution-Induced Surface Roughening and Oxygen Evolution Electrocatalysis of Alkaline-Earth Iridates in Acid. *Chem* **2019**, *5*, 3243–3259. [[CrossRef](#)]

61. Varsha, V.M.; Nageswaran, G. Operando X-Ray Spectroscopic Techniques: A Focus on Hydrogen and Oxygen Evolution Reactions. *Front. Chem.* **2020**, *8*, 23. [[CrossRef](#)]
62. Xu, Z.J. Transition metal oxides for water oxidation: All about oxyhydroxides? *Sci. China Mater.* **2019**, *63*, 3–7. [[CrossRef](#)]
63. Jiang, H.; He, Q.; Zhang, Y.; Song, L. Structural Self-Reconstruction of Catalysts in Electrocatalysis. *Acc. Chem. Res.* **2018**, *51*, 2968–2977. [[CrossRef](#)] [[PubMed](#)]
64. Liu, X.; Meng, J.; Zhu, J.; Huang, M.; Wen, B.; Guo, R.; Mai, L. Comprehensive Understandings into Complete Reconstruction of Precatalysts: Synthesis, Applications, and Characterizations. *Adv. Mater.* **2021**, *33*, 2007344. [[CrossRef](#)]
65. Li, S.; Li, Z.; Ma, R.; Gao, C.; Liu, L.; Hu, L.; Zhu, J.; Sun, T.; Tang, Y.; Liu, D.; et al. A Glass-Ceramic with Accelerated Surface Reconstruction toward the Efficient Oxygen Evolution Reaction. *Angew. Chem. Int. Ed.* **2021**, *60*, 3773–3780. [[CrossRef](#)]
66. Jiang, H.; He, Q.; Li, X.; Su, X.; Zhang, Y.; Chen, S.; Zhang, S.; Zhang, G.; Jiang, J.; Luo, Y.; et al. Tracking Structural Self-Reconstruction and Identifying True Active Sites toward Cobalt Oxychloride Precatalyst of Oxygen Evolution Reaction. *Adv. Mater.* **2019**, *31*, 1805127. [[CrossRef](#)] [[PubMed](#)]
67. Guan, D.; Ryu, G.; Hu, Z.; Zhou, J.; Dong, C.-L.; Huang, Y.-C.; Zhang, K.; Zhong, Y.; Komarek, A.C.; Zhu, M.; et al. Utilizing ion leaching effects for achieving high oxygen-evolving performance on hybrid nanocomposite with self-optimized behaviors. *Nat. Commun.* **2020**, *11*, 3376. [[CrossRef](#)]
68. Xu, X.; Su, C.; Shao, Z. Fundamental Understanding and Application of Ba_{0.5}Sr_{0.5}Co_{0.8}Fe_{0.2}O_{3-δ} Perovskite in Energy Storage and Conversion: Past, Present, and Future. *Energy Fuels* **2021**, *35*, 13585–13609. [[CrossRef](#)]
69. Suntivich, J.; May, K.J.; Gasteiger, H.A.; Goodenough, J.B.; Shao-Horn, Y. A Perovskite Oxide Optimized for Oxygen Evolution Catalysis from Molecular Orbital Principles. *Science* **2011**, *334*, 1383–1385. [[CrossRef](#)]
70. May, K.J.; Carlton, C.E.; Stoerzinger, K.A.; Risch, M.; Suntivich, J.; Lee, Y.-L.; Grimaud, A.; Shao-Horn, Y. Influence of Oxygen Evolution during Water Oxidation on the Surface of Perovskite Oxide Catalysts. *J. Phys. Chem. Lett.* **2012**, *3*, 3264–3270. [[CrossRef](#)]
71. Shen, T.-H.; Spillane, L.; Vavra, J.; Pham, T.H.M.; Peng, J.; Shao-Horn, Y.; Tileli, V. Oxygen Evolution Reaction in Ba_{0.5}Sr_{0.5}Co_{0.8}Fe_{0.2}O_{3-δ} Aided by Intrinsic Co/Fe Spinel-Like Surface. *J. Am. Chem. Soc.* **2020**, *142*, 15876–15883. [[CrossRef](#)]
72. Kim, B.J.; Fabbri, E.; Abbott, D.F.; Cheng, X.; Clark, A.H.; Nachttegaal, M.; Borlaf, M.; Castelli, I.E.; Graule, T.; Schmidt, T.J. Functional Role of Fe-Doping in Co-Based Perovskite Oxide Catalysts for Oxygen Evolution Reaction. *J. Am. Chem. Soc.* **2019**, *141*, 5231–5240. [[CrossRef](#)] [[PubMed](#)]
73. Wang, J.; Kim, S.-J.; Liu, J.; Gao, Y.; Choi, S.; Han, J.; Shin, H.; Jo, S.; Kim, J.; Ciucci, F.; et al. Redirecting dynamic surface restructuring of a layered transition metal oxide catalyst for superior water oxidation. *Nat. Catal.* **2021**, *4*, 212–222. [[CrossRef](#)]
74. Kim, M.; Park, J.; Ju, H.; Kim, J.Y.; Cho, H.-S.; Kim, C.-H.; Kim, B.-H.; Lee, S.W. Understanding synergistic metal–oxide interactions of in situ exsolved metal nanoparticles on a pyrochlore oxide support for enhanced water splitting. *Energy Environ. Sci.* **2021**, *14*, 3053–3063. [[CrossRef](#)]
75. Sun, H.; Zhou, W. Progress on X-ray Absorption Spectroscopy for the Characterization of Perovskite-Type Oxide Electrocatalysts. *Energy Fuels* **2021**, *35*, 5716–5737. [[CrossRef](#)]
76. Zhu, Y.; Kuo, T.-R.; Li, Y.-H.; Qi, M.-Y.; Chen, G.; Wang, J.; Xu, Y.-J.; Chen, H.M. Emerging Dynamic Structure of Electrocatalysts Unveiled by In Situ X-ray Diffraction/Absorption Spectroscopy. *Energy Environ. Sci.* **2021**, *14*, 1928–1958. [[CrossRef](#)]
77. Xiong, J.; Zhong, H.; Li, J.; Zhang, X.; Shi, J.; Cai, W.; Qu, K.; Zhu, C.; Yang, Z.; Beckman, S.P.; et al. Engineering highly active oxygen sites in perovskite oxides for stable and efficient oxygen evolution. *Appl. Catal. B Environ.* **2019**, *256*, 117817. [[CrossRef](#)]
78. Fan, K.; Zou, H.; Lu, Y.; Chen, H.; Li, F.; Liu, J.; Sun, L.; Tong, L.; Toney, M.F.; Sui, M.; et al. Direct Observation of Structural Evolution of Metal Chalcogenide in Electrocatalytic Water Oxidation. *ACS Nano* **2018**, *12*, 12369–12379. [[CrossRef](#)] [[PubMed](#)]
79. Li, Y.; Du, X.; Huang, J.; Wu, C.; Sun, Y.; Zou, G.; Yang, C.; Xiong, J. Recent Progress on Surface Reconstruction of Earth-Abundant Electrocatalysts for Water Oxidation. *Small* **2019**, *15*, 1901980. [[CrossRef](#)]
80. Garlyyev, B.; Liang, Y.; Xue, S.; Watzel, S.; Fichtner, J.; Li, W.-J.; Ding, X.; Bandarenka, A.S. Theoretical and experimental identification of active electrocatalytic surface sites. *Curr. Opin. Electrochem.* **2019**, *14*, 206–213. [[CrossRef](#)]
81. Xiong, Y.; Yang, Y.; Feng, X.; DiSalvo, F.J.; Abruna, H.D. A Strategy for Increasing the Efficiency of the Oxygen Reduction Reaction in Mn-Doped Cobalt Ferrites. *J. Am. Chem. Soc.* **2019**, *141*, 4412–4421. [[CrossRef](#)]
82. Zhu, Y.; Wang, J.; Chu, H.; Chu, Y.-C.; Chen, H.M. In Situ/Operando Studies for Designing Next-Generation Electrocatalysts. *ACS Energy Lett.* **2020**, *5*, 1281–1291. [[CrossRef](#)]
83. Sun, H.; Xu, X.; Yan, Z.; Chen, X.; Cheng, F.; Weiss, P.S.; Chen, J. Porous Multishelled Ni₂P Hollow Microspheres as an Active Electrocatalyst for Hydrogen and Oxygen Evolution. *Chem. Mater.* **2017**, *29*, 8539–8547. [[CrossRef](#)]
84. Zhang, B.; Jiang, K.; Wang, H.; Hu, S. Fluoride-Induced Dynamic Surface Self-Reconstruction Produces Unexpectedly Efficient Oxygen-Evolution Catalyst. *Nano Lett.* **2019**, *19*, 530–537. [[CrossRef](#)]
85. Liu, X.; Meng, J.; Ni, K.; Guo, R.; Xia, F.; Xie, J.; Li, X.; Wen, B.; Wu, P.; Li, M.; et al. Complete Reconstruction of Hydrate Pre-Catalysts for Ultrastable Water Electrolysis in Industrial-Concentration Alkali Media. *Cell Rep. Phys. Sci.* **2020**, *1*, 100241. [[CrossRef](#)]
86. Polo-Garzon, F.; Bao, Z.; Zhang, X.; Huang, W.; Wu, Z. Surface Reconstructions of Metal Oxides and the Consequences on Catalytic Chemistry. *ACS Catal.* **2019**, *9*, 5692–5707. [[CrossRef](#)]
87. Selvam, N.C.S.; Du, L.; Xia, B.Y.; Yoo, P.J.; You, B. Reconstructed Water Oxidation Electrocatalysts: The Impact of Surface Dynamics on Intrinsic Activities. *Adv. Funct. Mater.* **2020**, *31*, 2008190. [[CrossRef](#)]

88. Jiang, W.-J.; Tang, T.; Zhang, Y.; Hu, J.-S. Synergistic Modulation of Non-Precious-Metal Electrocatalysts for Advanced Water Splitting. *Acc. Chem. Res.* **2020**, *53*, 1111–1123. [[CrossRef](#)] [[PubMed](#)]
89. Lee, K.; Osada, M.; Hwang, H.Y.; Hikita, Y. Oxygen Evolution Reaction Activity in IrO_x/SrIrO₃ Catalysts: Correlations between Structural Parameters and the Catalytic Activity. *J. Phys. Chem. Lett.* **2019**, *10*, 1516–1522. [[CrossRef](#)] [[PubMed](#)]
90. Ge, R.; Li, L.; Su, J.; Lin, Y.; Tian, Z.; Chen, L. Ultrafine Defective RuO₂ Electrocatalyst Integrated on Carbon Cloth for Robust Water Oxidation in Acidic Media. *Adv. Energy Mater.* **2019**, *9*, 1901313. [[CrossRef](#)]
91. Lin, Y.; Tian, Z.; Zhang, L.; Ma, J.; Jiang, Z.; Deibert, B.J.; Ge, R.; Chen, L. Chromium-ruthenium oxide solid solution electrocatalyst for highly efficient oxygen evolution reaction in acidic media. *Nat. Commun.* **2019**, *10*, 162. [[CrossRef](#)]
92. Duan, Y.; Sun, S.; Sun, Y.; Xi, S.; Chi, X.; Zhang, Q.; Ren, X.; Wang, J.; Ong, S.J.H.; Du, Y.; et al. Mastering Surface Reconstruction of Metastable Spinel Oxides for Better Water Oxidation. *Adv. Mater.* **2019**, *31*, e1807898. [[CrossRef](#)]
93. Zhou, J.; Zhang, L.; Huang, Y.-C.; Dong, C.-L.; Lin, H.-J.; Chen, C.-T.; Tjeng, L.H.; Hu, Z. Voltage- and time-dependent valence state transition in cobalt oxide catalysts during the oxygen evolution reaction. *Nat. Commun.* **2020**, *11*, 1984. [[CrossRef](#)]
94. Chang, C.-J.; Zhu, Y.; Wang, J.; Chen, H.-C.; Tung, C.-W.; Chu, Y.-C.; Chen, H.M. In situ X-ray diffraction and X-ray absorption spectroscopy of electrocatalysts for energy conversion reactions. *J. Mater. Chem. A* **2020**, *8*, 19079–19112. [[CrossRef](#)]
95. Yang, Y.; Wang, Y.; Xiong, Y.; Huang, X.; Shen, L.; Huang, R.; Wang, H.; Pastore, J.P.; Yu, S.-H.; Xiao, L.; et al. In Situ X-ray Absorption Spectroscopy of a Synergistic Co–Mn Oxide Catalyst for the Oxygen Reduction Reaction. *J. Am. Chem. Soc.* **2019**, *141*, 1463–1466. [[CrossRef](#)]
96. Wang, M.; Árnadóttir, L.; Xu, Z.J.; Feng, Z. In Situ X-ray Absorption Spectroscopy Studies of Nanoscale Electrocatalysts. *Nano-Micro Lett.* **2019**, *11*, 47. [[CrossRef](#)] [[PubMed](#)]
97. Sun, H.; Hu, B.; Guan, D.; Hu, Z.; Fei, L.; Li, M.; Peterson, V.K.; Lin, H.-J.; Chen, C.-T.; Ran, R.; et al. Bulk and Surface Properties Regulation of Single/Double Perovskites to Realize Enhanced Oxygen Evolution Reactivity. *ChemSusChem* **2020**, *13*, 3045–3052. [[CrossRef](#)]
98. Zheng, X.; Zhang, B.; De Luna, P.; Liang, Y.; Comin, R.; Voznyy, O.; Han, L.; Garcia de Arquer, F.P.; Liu, M.; Dinh, C.T.; et al. Theory-driven design of high-valence metal sites for water oxidation confirmed using in situ soft X-ray absorption. *Nat. Chem.* **2018**, *10*, 149–154. [[CrossRef](#)] [[PubMed](#)]
99. Chen, S.; Huang, H.; Jiang, P.; Yang, K.; Diao, J.; Gong, S.; Liu, S.; Huang, M.; Wang, H.; Chen, Q. Mn-Doped RuO₂ Nanocrystals as Highly Active Electrocatalysts for Enhanced Oxygen Evolution in Acidic Media. *ACS Catal.* **2020**, *10*, 1152–1160. [[CrossRef](#)]
100. Wang, J.; Ji, Y.; Yin, R.; Li, Y.; Shao, Q.; Huang, X. Transition metal-doped ultrathin RuO₂ networked nanowires for efficient overall water splitting across a broad pH range. *J. Mater. Chem. A* **2019**, *7*, 6411–6416. [[CrossRef](#)]
101. Wang, C.; Qi, L. Heterostructured Inter-Doped Ruthenium–Cobalt Oxide Hollow Nanosheet Arrays for Highly Efficient Overall Water Splitting. *Angew. Chem. Int. Ed.* **2020**, *59*, 17219–17224. [[CrossRef](#)] [[PubMed](#)]
102. Hao, S.; Liu, M.; Pan, J.; Liu, X.; Tan, X.; Xu, N.; He, Y.; Lei, L.; Zhang, X. Dopants fixation of Ruthenium for boosting acidic oxygen evolution stability and activity. *Nat. Commun.* **2020**, *11*, 5368. [[CrossRef](#)] [[PubMed](#)]
103. Tong, Y.; Wu, J.; Chen, P.; Liu, H.; Chu, W.; Wu, C.; Xie, Y. Vibronic Superexchange in Double Perovskite Electrocatalyst for Efficient Electrocatalytic Oxygen Evolution. *J. Am. Chem. Soc.* **2018**, *140*, 11165–11169. [[CrossRef](#)]
104. Wu, T.; Sun, S.; Song, J.; Xi, S.; Du, Y.; Chen, B.; Sasangka, W.A.; Liao, H.; Gan, C.L.; Scherer, G.G.; et al. Iron-facilitated dynamic active-site generation on spinel CoAl₂O₄ with self-termination of surface reconstruction for water oxidation. *Nat. Catal.* **2019**, *2*, 763–772. [[CrossRef](#)]
105. Kim, M.; Lee, B.; Ju, H.; Kim, J. Reducing the Barrier Energy of Self-Reconstruction for Anchored Cobalt Nanoparticles as Highly Active Oxygen Evolution Electrocatalyst. *Adv. Mater.* **2019**, *31*, 1901977. [[CrossRef](#)]
106. Li, X.; Wang, H.; Cui, Z.; Li, Y.; Xin, S.; Zhou, J.; Long, Y.; Jin, C.; Goodenough, J.B. Exceptional oxygen evolution reactivities on CaCoO₃ and SrCoO₃. *Sci. Adv.* **2019**, *5*, eaav6262. [[CrossRef](#)]
107. Wang, H.; Wu, J.; Dolocan, A.; Li, Y.; Lu, X.; Wu, N.; Park, K.; Xin, S.; Lei, M.; Yang, W.; et al. Short O–O separation in layered oxide Na_{0.67}CoO₂ enables an ultrafast oxygen evolution reaction. *Proc. Natl. Acad. Sci. USA* **2019**, *116*, 23473–23479. [[CrossRef](#)]
108. Zhu, Y.; Tahini, H.A.; Hu, Z.; Chen, Z.-G.; Zhou, W.; Komarek, A.C.; Lin, Q.; Lin, H.-J.; Chen, C.-T.; Zhong, Y.; et al. Boosting Oxygen Evolution Reaction by Creating Both Metal Ion and Lattice-Oxygen Active Sites in a Complex Oxide. *Adv. Mater.* **2020**, *32*, 1905025. [[CrossRef](#)]
109. Yagi, S.; Yamada, I.; Tsukasaki, H.; Seno, A.; Murakami, M.; Fujii, H.; Chen, H.; Umezawa, N.; Abe, H.; Nishiyama, N.; et al. Covalency-reinforced oxygen evolution reaction catalyst. *Nat. Commun.* **2015**, *6*, 8249. [[CrossRef](#)]
110. Zhang, R.; Dubouis, N.; Ben Osman, M.; Yin, W.; Sougrati, M.T.; Corte, D.A.D.; Giaume, D.; Grimaud, A. A Dissolution/Precipitation Equilibrium on the Surface of Iridium-Based Perovskites Controls Their Activity as Oxygen Evolution Reaction Catalysts in Acidic Media. *Angew. Chem. Int. Ed.* **2019**, *58*, 4571–4575. [[CrossRef](#)]
111. Zhu, Y.; Tahini, H.A.; Hu, Z.; Dai, J.; Chen, Y.; Sun, H.; Zhou, W.; Liu, M.; Smith, S.C.; Wang, H.; et al. Unusual synergistic effect in layered Ruddlesden–Popper oxide enables ultrafast hydrogen evolution. *Nat. Commun.* **2019**, *10*, 149. [[CrossRef](#)]
112. Yu, J.; Wu, X.; Guan, D.; Hu, Z.; Weng, S.-C.; Sun, H.; Song, Y.; Ran, R.; Zhou, W.; Ni, M.; et al. Monoclinic SrIrO₃: An Easily Synthesized Conductive Perovskite Oxide with Outstanding Performance for Overall Water Splitting in Alkaline Solution. *Chem. Mater.* **2020**, *32*, 4509–4517. [[CrossRef](#)]

113. Duan, Y.; Lee, J.Y.; Xi, S.; Sun, Y.; Ge, J.; Ong, S.J.H.; Chen, Y.; Dou, S.; Meng, F.; Diao, C.; et al. Anodic Oxidation Enabled Cation Leaching for Promoting Surface Reconstruction in Water Oxidation. *Angew. Chem. Int. Ed.* **2021**, *60*, 7418–7425. [[CrossRef](#)] [[PubMed](#)]
114. Xu, Q.; Jiang, H.; Duan, X.; Jiang, Z.; Hu, Y.; Boettcher, S.W.; Zhang, W.; Guo, S.; Li, C. Fluorination-enabled Reconstruction of NiFe Electrocatalysts for Efficient Water Oxidation. *Nano Lett.* **2021**, *21*, 492–499. [[CrossRef](#)]
115. Xu, Q.; Chu, M.; Liu, M.; Zhang, J.; Jiang, H.; Li, C. Fluorine-triggered surface reconstruction of Ni₃S₂ electrocatalysts towards enhanced water oxidation. *Chem. Eng. J.* **2021**, *411*, 128488. [[CrossRef](#)]
116. Zhang, S.; Yu, T.; Wen, H.; Ni, Z.; He, Y.; Guo, R.; You, J.; Liu, X. The latest development of CoOOH two-dimensional materials used as OER catalysts. *Chem. Commun.* **2020**, *56*, 15387–15405. [[CrossRef](#)]
117. Zhou, Y.-N.; Li, M.-X.; Dou, S.-Y.; Wang, H.-Y.; Dong, B.; Liu, H.-J.; Zhao, H.-Y.; Wang, F.-L.; Yu, J.-F.; Chai, Y.-M. Promoting Oxygen Evolution by Deep Reconstruction via Dynamic Migration of Fluorine Anions. *ACS Appl. Mater. Interfaces* **2021**, *13*, 34438–34446. [[CrossRef](#)] [[PubMed](#)]
118. Yan, P.; Liu, Q.; Zhang, H.; Qiu, L.; Wu, H.B.; Yu, X.-Y. Deeply reconstructed hierarchical and defective NiOOH/FeOOH nanoboxes with accelerated kinetics for the oxygen evolution reaction. *J. Mater. Chem. A* **2021**, *9*, 15586–15594. [[CrossRef](#)]
119. Wang, Y.; Zhu, Y.; Zhao, S.; She, S.; Selomulya, C.J.M. Anion Etching for Accessing Rapid and Deep Self-Reconstruction of Precatalysts for Water Oxidation. *Matter* **2020**, *3*, 2124–2137. [[CrossRef](#)]
120. Chatti, M.; Gardiner, J.L.; Fournier, M.; Johannessen, B.; Williams, T.; Gengenbach, T.R.; Pai, N.; Nguyen, C.; MacFarlane, D.R.; Hocking, R.K.; et al. Intrinsically stable in situ generated electrocatalyst for long-term oxidation of acidic water at up to 80 °C. *Nat. Catal.* **2019**, *2*, 457–465. [[CrossRef](#)]
121. Huang, Z.-F.; Song, J.; Du, Y.; Xi, S.; Dou, S.; Nsanzimana, J.M.V.; Wang, C.; Xu, Z.J.; Wang, X. Chemical and structural origin of lattice oxygen oxidation in Co–Zn oxyhydroxide oxygen evolution electrocatalysts. *Nat. Energy* **2019**, *4*, 329–338. [[CrossRef](#)]
122. Zhou, J.; Wang, Y.; Su, X.; Gu, S.; Liu, R.; Huang, Y.; Yan, S.; Li, J.; Zhang, S. Electrochemically accessing ultrathin Co (oxy)-hydroxide nanosheets and operando identifying their active phase for the oxygen evolution reaction. *Energy Environ. Sci.* **2019**, *12*, 739–746. [[CrossRef](#)]
123. Kim, J.-H.; Kawashima, K.; Wygant, B.R.; Mabayoje, O.; Liu, Y.; Wang, J.H.; Mullins, C.B. Transformation of a Cobalt Carbide (Co₃C) Oxygen Evolution Precatalyst. *ACS Appl. Energy Mater.* **2018**, *1*, 5145–5150. [[CrossRef](#)]
124. Bergmann, A.; Martinez-Moreno, E.; Teschner, D.; Chernev, P.; Gliech, M.; de Araújo, J.F.; Reier, T.; Dau, H.; Strasser, P. Reversible amorphization and the catalytically active state of crystalline Co₃O₄ during oxygen evolution. *Nat. Commun.* **2015**, *6*, 8625. [[CrossRef](#)] [[PubMed](#)]
125. Xiao, Z.; Huang, Y.-C.; Dong, C.-L.; Xie, C.; Liu, Z.; Du, S.; Chen, W.; Yan, D.; Tao, L.; Shu, Z.; et al. Operando Identification of the Dynamic Behavior of Oxygen Vacancy-rich Co₃O₄ for Oxygen Evolution Reaction. *J. Am. Chem. Soc.* **2020**, *142*, 12087–12095. [[CrossRef](#)] [[PubMed](#)]
126. Chen, Y.; Li, H.; Wang, J.; Du, Y.; Xi, S.; Sun, Y.; Sherburne, M.; Ager, J.W.; Fisher, A.C.; Xu, Z.J. Exceptionally active iridium evolved from a pseudo-cubic perovskite for oxygen evolution in acid. *Nat. Commun.* **2019**, *10*, 572. [[CrossRef](#)]
127. Zagalskaya, A.; Alexandrov, V. Mechanistic Study of IrO₂ Dissolution during the Electrocatalytic Oxygen Evolution Reaction. *J. Phys. Chem. Lett.* **2020**, *11*, 2695–2700. [[CrossRef](#)]
128. Zhang, S.; Gu, S.; Wang, Y.; Liang, C.; Yu, Y.; Han, L.; Zheng, S.; Zhang, N.; Liu, X.; Zhou, J.; et al. Spontaneous Delithiation under Operando Condition Triggers Formation of an Amorphous Active Layer in Spinel Cobalt Oxides Electrocatalyst toward Oxygen Evolution. *ACS Catal.* **2019**, *9*, 7389–7397. [[CrossRef](#)]
129. Liu, H.; Yang, L.; Qiao, K.; Zeng, X.; Huang, Y.; Zheng, L.; Cao, D. A new concept analogous to homogeneous catalysis to construct in-situ regenerative electrodes for long-term oxygen evolution reaction. *Nano Energy* **2020**, *76*, 105115. [[CrossRef](#)]
130. Feng, K.; Zhang, D.; Liu, F.; Li, H.; Xu, J.; Xia, Y.; Li, Y.; Lin, H.; Wang, S.; Shao, M.; et al. Highly Efficient Oxygen Evolution by a Thermocatalytic Process Cascaded Electrocatalysis Over Sulfur-Treated Fe-Based Metal–Organic-Frameworks. *Adv. Energy Mater.* **2020**, *10*, 2000184. [[CrossRef](#)]
131. Che, Q.; Li, Q.; Tan, Y.; Chen, X.; Xu, X.; Chen, Y. One-step controllable synthesis of amorphous (Ni-Fe)_x/NiFe(OH)_y hollow microtube/sphere films as superior bifunctional electrocatalysts for quasi-industrial water splitting at large-current-density. *Appl. Catal. B Environ.* **2019**, *246*, 337–348. [[CrossRef](#)]
132. Xu, Y.; Wang, C.; Huang, Y.; Fu, J. Recent advances in electrocatalysts for neutral and large-current-density water electrolysis. *Nano Energy* **2021**, *80*, 105545. [[CrossRef](#)]
133. Zhang, L.; Wang, X.; Li, A.; Zheng, X.; Peng, L.; Huang, J.; Deng, Z.; Chen, H.; Wei, Z. Rational construction of macroporous CoFeP triangular plate arrays from bimetal–organic frameworks as high-performance overall water-splitting catalysts. *J. Mater. Chem. A* **2019**, *7*, 17529–17535. [[CrossRef](#)]
134. Duan, Y.; Sun, S.; Xi, S.; Ren, X.; Zhou, Y.; Zhang, G.; Yang, H.; Du, Y.; Xu, Z.J. Tailoring the Co 3d-O 2p Covalency in LaCoO₃ by Fe Substitution To Promote Oxygen Evolution Reaction. *Chem. Mater.* **2017**, *29*, 10534–10541. [[CrossRef](#)]
135. Huang, X.; Wang, J.; Tao, H.B.; Tian, H.; Xu, H. An essential descriptor for the oxygen evolution reaction on reducible metal oxide surfaces. *Chem. Sci.* **2019**, *10*, 3340–3345. [[CrossRef](#)]
136. Huang, H.-C.; Zhao, Y.; Wang, J.; Li, J.; Chen, J.; Fu, Q.; Bu, Y.-X.; Cheng, S.-B. Rational design of an efficient descriptor for single-atom catalysts in the hydrogen evolution reaction. *J. Mater. Chem. A* **2020**, *8*, 9202–9208. [[CrossRef](#)]

137. Wang, X.; Gao, X.J.; Qin, L.; Wang, C.; Song, L.; Zhou, Y.-N.; Zhu, G.; Cao, W.; Lin, S.; Zhou, L.; et al. e_g occupancy as an effective descriptor for the catalytic activity of perovskite oxide-based peroxidase mimics. *Nat. Commun.* **2019**, *10*, 704. [[CrossRef](#)]
138. Fan, Z.; Zhang, L.; Baumann, D.; Mei, L.; Yao, Y.; Duan, X.; Shi, Y.; Huang, J.; Huang, Y.; Duan, X. In Situ Transmission Electron Microscopy for Energy Materials and Devices. *Adv. Mater.* **2019**, *31*, 1900608. [[CrossRef](#)]
139. Liu, D.; Shadik, Z.; Lin, R.; Qian, K.; Li, H.; Li, K.; Wang, S.; Yu, Q.; Liu, M.; Ganapathy, S.; et al. Review of Recent Development of In Situ/Operando Characterization Techniques for Lithium Battery Research. *Adv. Mater.* **2019**, *31*, 1806620. [[CrossRef](#)]
140. Li, L.; Sun, H.; Hu, Z.; Zhou, J.; Huang, Y.-C.; Huang, H.; Song, S.; Pao, C.-W.; Chang, Y.-C.; Komarek, A.C.; et al. In Situ/Operando Capturing Unusual Ir^{6+} Facilitating Ultrafast Electrocatalytic Water Oxidation. *Adv. Funct. Mater.* **2021**, 2104746. [[CrossRef](#)]
141. Dai, S.; Zhang, Z.; Xu, J.; Shen, W.; Zhang, Q.; Yang, X.; Xu, T.; Dang, D.; Hu, H.; Zhao, B.; et al. In situ Raman study of nickel bicarbonate for high-performance energy storage device. *Nano Energy* **2019**, *64*, 103919. [[CrossRef](#)]
142. Li, X.; Yang, X.; Zhang, J.; Huang, Y.; Liu, B. In Situ/Operando Techniques for Characterization of Single-Atom Catalysts. *ACS Catal.* **2019**, *9*, 2521–2531. [[CrossRef](#)]
143. Zhu, Y.; Chen, H.-C.; Hsu, C.-S.; Lin, T.-S.; Chang, C.-J.; Chang, S.-C.; Tsai, L.-D.; Chen, H.M. Operando Unraveling of the Structural and Chemical Stability of P-Substituted CoSe_2 Electrocatalysts toward Hydrogen and Oxygen Evolution Reactions in Alkaline Electrolyte. *ACS Energy Lett.* **2019**, *4*, 987–994. [[CrossRef](#)]
144. Andronesco, C.; Seisel, S.; Wilde, P.; Barwe, S.; Masa, J.; Chen, Y.-T.; Ventosa, E.; Schuhmann, W. Influence of Temperature and Electrolyte Concentration on the Structure and Catalytic Oxygen Evolution Activity of Nickel–Iron Layered Double Hydroxide. *Chem. Eur. J.* **2018**, *24*, 13773–13777. [[CrossRef](#)] [[PubMed](#)]